Fractional quantum Hall bilayers at half filling: Tunneling-driven non-Abelian phase

W. Zhu,[1] Zhao Liu,[2] F. D. M. Haldane,[3] and D. N. Sheng[1]

[1]*Department of Physics and Astronomy, California State University, Northridge, California 91330, USA*

[2]*Dahlem Center for Complex Quantum Systems and Institut für Theoretische Physik, Freie Universität Berlin, Arnimallee 14, 14195 Berlin, Germany*

[3]*Department of Physics, Princeton University, Princeton, New Jersey 08544, USA*

(Received 17 September 2016; revised manuscript received 14 December 2016; published 30 December 2016)

Multicomponent quantum Hall systems with internal degrees of freedom provide a fertile ground for the emergence of exotic quantum liquids. Here, we investigate the possibility of non-Abelian topological order in the half-filled fractional quantum Hall (FQH) bilayer system driven by the tunneling effect between two layers. By means of the state-of-the-art density-matrix renormalization group, we unveil "fingerprint" evidence of the non-Abelian Moore-Read Pfaffian state emerging in the intermediate-tunneling regime, including the ground-state degeneracy on the torus geometry and the topological entanglement spectroscopy (entanglement spectrum and topological entanglement entropy) on the spherical geometry, respectively. Remarkably, the phase transition from the previously identified Abelian (331) Halperin state to the non-Abelian Moore-Read Pfaffian state is determined to be continuous, which is signaled by the continuous evolution of the universal part of the entanglement spectrum, and discontinuities in the excitation gap and the derivative of the ground-state energy. Our results not only provide a "proof-of-principle" demonstration of realizing a non-Abelian state through coupling different degrees of freedom, but also open up a possibility in FQH bilayer systems for detecting different chiral p-wave pairing states.

DOI: 10.1103/PhysRevB.94.245147

I. INTRODUCTION

When two-dimensional electron systems subject to a strong magnetic field, electron-electron interactions can drive transitions into a series of remarkable quantum states of matter, dubbed as fractional quantum Hall (FQH) effect [1,2]. The FQH effect is an example of the topological state of matter [3], providing a spectacular platform for anyonic statistics in two dimensions: the emergent excitations carry fractionalized quantum numbers and obey Abelian [2] or non-Abelian quantum statistics [4–6]. Among them, the non-Abelian FQH effect is expected to form the substrate for topological quantum computation [7], thus is of great importance. Albeit vigorous research efforts [8–13], to date convincing experimental evidence of non-Abelian FQH states is still rare, with $\nu = \frac{5}{2}$ and $\frac{12}{5}$ as two prominent examples realized in single-component FQH systems. Compared to single-component systems, multicomponent FQH systems with extra degrees of freedom offer additional tunable parameters and allow the observation of richer quantum phase diagrams [14–18]. The internal degrees of freedom correspond to realistic experimental circumstances, for example, layers, subbands, or spins in GaAs quantum wells (QWs) [19–23], spins or valleys in graphene or AlAs, which lead to effective multilayers separated by layer distance d with electrons' tunneling $t_\perp$ between layers (Fig. 1). Two most notable examples of the multicomponent FQH effects are the observation of quantized Hall plateaus at total filling factors $\nu_T = \frac{1}{2}$ and $\nu_T = 1$ in double QW and wide QW systems. The $\nu_T = 1$ state [23] is believed to favor a symmetry-breaking state with spontaneous interlayer phase coherence, which induces a remarkable exciton condensation. The $\nu_T = \frac{1}{2}$ state [19–22] has turned out to be more interesting and controversial, as it can be an Abelian Halperin FQH state, but also be a possible platform for realizing non-Abelian anyonic statistics, which has been pursued persistently in the past [16–18,24–31].

In this paper, we consider a two-component FQH system with N_e electrons (as illustrated in Fig. 1) described by the following realistic Hamiltonian containing essential information relevant to experiments:

$$H = \sum_{i<j}^{N_e}[V_{\uparrow\uparrow}(|\mathbf{r}_{i\uparrow} - \mathbf{r}_{j\uparrow}|) + V_{\downarrow\downarrow}(|\mathbf{r}_{i\downarrow} - \mathbf{r}_{j\downarrow}|)] + \sum_{i,j}^{N_e} V_{\uparrow\downarrow}(|\mathbf{r}_{i\uparrow} - \mathbf{r}_{j\downarrow}|) + H_t, \quad (1)$$

where we label two layers by index $\sigma \in \{\uparrow, \downarrow\}$ and the position of the ith electron in layer σ by $\mathbf{r}_{i\sigma}$. $V_{\uparrow\uparrow}(r) = V_{\downarrow\downarrow}(r)$ is the Coulomb potential in a single layer with finite width w, and $V_{\uparrow\downarrow}(r)$ is the interlayer Coulomb interaction incorporating finite interlayer separation d. H_t is the electron tunneling of strength $t_\perp$ between two layers. For numerical convenience, we choose the lowest Landau level (LLL) orbital basis to do the second quantization of the above Hamiltonian (see Appendix A for details), where the tunneling term can be written as $H_t = -t_\perp \sum_{m=0}^{N_s-1}(c^\dagger_{m,\uparrow}c_{m,\downarrow} + c^\dagger_{m,\downarrow}c_{m,\uparrow})$. Here, $c^\dagger_{m,\sigma}$ ($c_{m,\sigma}$) is the creation (annihilation) operator of an electron in the LLL orbital m of layer σ, and N_s is total number of orbitals in each layer. We focus on the total filling $\nu_T = N_e/N_s = \frac{1}{2}$ throughout this work, and use the magnetic length ℓ and the Coulomb energy e^2/ℓ as the units of length and energy, respectively, where $-e$ is the electron charge.

In limits of the spatial separation $d \to 0$ and $d \to \infty$, the bilayer ground states at $\nu_T = \frac{1}{2}$ are compressible because either the single-layer limit ($d \to 0$) or the two-isolated-layer limit ($d \to \infty$) can be well understood by the "composite Fermi liquid" (CFL) theory [32]. In the intermediate regime $d \sim 2$–6, the incompressibility of the system is observed in various experiments [19–22]. However, its precise origin is still

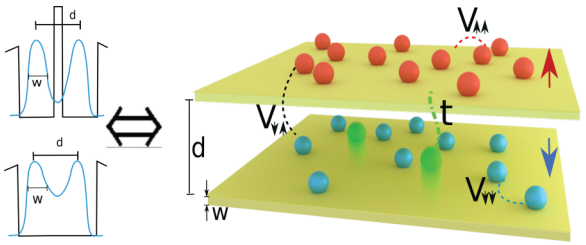

FIG. 1. A schematic diagram for the FQH bilayer system. Both double QW and single wide QW systems can be mapped to a bilayer system, where electrons interact with each other through intralayer interaction $V_{\sigma\sigma}$ and interlayer interaction $V_{\sigma\bar{\sigma}}$, and the electron tunneling $t_\perp$ is tunable between two separated layers.

a long-standing subject. Numerical simulations [33–36] have confirmed that the Abelian (331) Halperin state dominates at vanishing interlayer tunneling ($t_\perp = 0$) [14]. Remarkably, through uncovering the underlying pairing nature of the (331) Halperin state [24,25], it has been suggested that the tunneling effect may drive the system into a non-Abelian phase [16–18,26–31], which motivates intensive efforts [36–40] to establish its existence. However, previous numerical studies, primarily utilizing exact diagonalization on small system sizes, are still too limited to reach a consensus. For instance, the only evidence of a non-Abelian phase was obtained by simply comparing the Coulomb ground state with the trial wave function [38]. On the contrary, subsequent studies even suggest that the CFL [39] and the (331) Halperin state [36] may still dominate at finite tunneling. Taken as a whole, to date, the possibility of realizing a non-Abelian state through coupling different degrees of freedom or tuning experimental relevant interactions remains elusive for the $\nu_T = \frac{1}{2}$ bilayer system, which urgently calls for revisiting this problem using state-of-the-art techniques [41–45].

In this paper, we uncover the nature of quantum states and determine the phase diagram for the FQH bilayer system at $\nu_T = \frac{1}{2}$ by means of large-scale density-matrix renormalization group (DMRG) [41–45] and exact diagonalization (ED) calculations. The system turns out to host two different incompressible liquid phases: one is the Abelian (331) Halperin state, and the other is the non-Abelian Moore-Read (MR) Pfaffian state, as identified by their different ground-state degeneracies on torus geometry. Remarkably, we demonstrate that they share the same topological entanglement entropy, but have different characteristic entanglement spectra on the spherical geometry. Furthermore, we identify a continuous phase transition between these two FQH phases driven by varying the tunneling strength $t_\perp$, reflected by the smooth evolution of the ground-state energy, and discontinuities of the excitation gap and the derivative of the ground-state energy. Intriguingly, our fingerprint evidence leads to two conclusions related to existing theories and experiments. First, the MR Pfaffian state can indeed be obtained by coupling different degrees of freedom. Although such a possibility was predicted about 20 years ago [16–18,24–27], convincing and comprehensive evidence directly from a microscopic description was missed until our work. Second, the previously found FQH $\nu_T = \frac{1}{2}$ plateau in single wide QW experiments [19,21,22], where the tunneling strength is taken to be considerable, *is most likely to* be captured by the MR Pfaffian state and in favor of a nontrivial $p_x + ip_y$ pairing mechanism. By reducing the effective tunneling (through tuning electron density), the system undergoes a transition from the non-Abelian MR Pfaffian to the weak p-wave pairing (331) Halperin state, while the Hall conductance keeps unchanged. Thus, the $\nu_T = \frac{1}{2}$ bilayer system provides a promising platform for realizing different $p_x + ip_y$ pairing physics through coupling different degrees of freedom [46–48] within experimentally attainable parameters. We believe our work paves the way for future research realizing new classes of non-Abelian states in realistic bilayer systems. Specific measurements for identifying the bilayer non-Abelian state in experiments are also discussed.

II. ENERGY SPECTRUM

We first investigate the torus geometry with periodic boundary condition, where different topological states can be distinguished by their ground-state degeneracies. At filling factor $\nu_T = \frac{1}{2}$, apart from a twofold degeneracy coming from the center-of-mass motion, there can be additional degeneracy occurring due to the multicomponent or the topological nature of the state, which is fourfold for the (331) Halperin state, and threefold for the MR Pfaffian state [5]. Here, we will inspect the low-energy spectrum as a function of the tunneling strength using DMRG.

In Fig. 2(a), we show the results for $N_e = 12$ electrons obtained by DMRG at layer width $w = 1.5$ and layer distance $d = 3.0$, where the degeneracy due to the center-of-mass motion has been excluded. When the tunneling is weak ($t_\perp < 0.04$), we identify the multiplet of four ground states in the spectrum as a signal of the (331) Halperin state. With the increasing of the tunneling strength, the fourfold

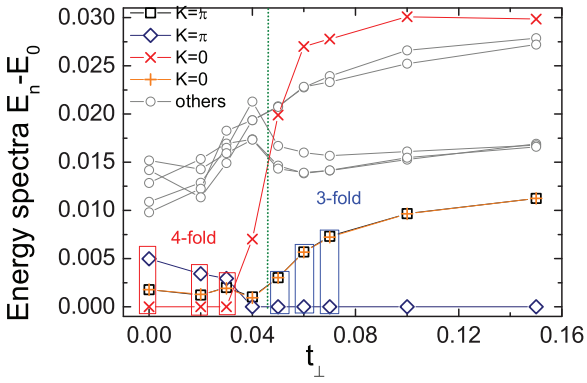

FIG. 2. Energy spectra as a function of the tunneling strength $t_\perp$, obtained on a square torus with $N_e = 12$ electrons by DMRG. Different momentum sectors are labeled by different symbols. We highlight the ground-state degeneracy by boxes. Here, we only show two lowest-energy levels in $K = 0$ (red cross, orange star) and $K = \pi$ (black square, navy diamond) sectors, and one lowest-energy level in other momentum sectors. Due to the C_4 symmetry on the square torus, one ground state in the $K = 0$ sector (orange star) has the nearly the same energy with one in the $K = \pi$ sector (black square). The dashed line marks the level crossing between the ground state in the $K = 0$ sector (red cross) and high excited states, indicating a quantum phase transition. All calculations are performed at layer distance $d = 3.0$ and layer width $w = 1.5$.

ground-state degeneracy is gradually destroyed. One state with momentum $K = 0$ (marked as red cross) is being gapped out for sufficiently large $t_\perp$, leaving the other three states in the ground-state manifold. Importantly, we find a region ($t_\perp > 0.04$) where the correct threefold MR Pfaffian degeneracy is visible, despite a finite-energy splitting among the three ground states. Here, we would like to point out, working on the larger system sizes is the key to reach this exciting result. In the system size $N_e < 12$, one energy state from $K \neq 0,\pi$ comes down and eventually forms a gapless branch in the low-energy spectrum (Appendix E), which prevents previous work [39] from reaching a positive conclusion of the threefold MR Pfaffian degeneracy.

III. ENTANGLEMENT SPECTROSCOPY

To uncover the topological nature of different quantum phases, we move to the spherical geometry, and perform the entanglement-based diagnosis. This geometry is commonly used for accessing larger systems as the unique ground state (selected by the finite-size shift, see Appendix A) on the sphere facilitates the computation task. We analyze the topological entanglement entropy (TEE) [49,50] and the entanglement spectrum (ES) [51] in different tunneling regimes with different ground-state degeneracies on the torus, and demonstrate that they accurately match the predictions for the (331) Halperin state and the MR Pfaffian state in the weak- and intermediate-tunneling regime, respectively. Importantly, all characterizations of phases are robust and stable for various system sizes [from $N_e = 14$ to 24 (see Appendix C)].

A. Topological entanglement entropy

The entanglement entropy of a bipartite quantum state $|\Psi\rangle_{AB}$ is defined as $S_A = -\mathrm{Tr}\rho_A \ln \rho_A$, where $\rho_A = \mathrm{Tr}_B(|\Psi\rangle\langle\Psi|)$ is the reduced density matrix of the subsystem A. For a gapped topological order in two dimensions, the area law $S_A = \alpha|\partial A| - \gamma$ holds, where $|\partial A|$ is the boundary length of the subsystem A, and the TEE γ is related to the total quantum dimension $\mathcal{D}$ by $\gamma = \ln \mathcal{D}$ [49,50]. Since $\mathcal{D}$ contains the information about quasiparticles, the TEE can determine whether a topological phase belongs to the universality class of a given topological field theory.

We make two identical single cuts, each applied to one sphere in our bilayer system, to divide all Landau level orbitals into two parts. The subsystem A contains $2l_A$ Landau level orbitals in total (l_A consecutive orbitals in each northern hemisphere). For partitions with different l_A, since the boundary length of the cut is proportional to $\sqrt{l_A}$, we expect the area law $S_A(l_A) = \alpha\sqrt{l_A} - \gamma$. Figures 3(a) and 3(d) show the numerically calculated orbital-cut entanglement entropy S_A (l_A) as a function of $\sqrt{l_A}$ for tunneling strength $t_\perp = 0.03$ and 0.10 at layer width $w = 1.5$ and layer distance $d = 3.0$. First of all, the approximately linear part of $S(l_A)$ shows a negative intercept in the limit of $l_A \to 0$, indicating a nonzero TEE. Through the finite-size scaling (red line) based on the raw data of $N_e = 22$, we extract the TEE as $\gamma \approx 1.119 \pm 0.143$ and $\gamma \approx 1.031 \pm 0.074$ for $t_\perp = 0.03$ and 0.10, respectively. Interestingly, the (331) Halperin state and the MR Pfaffian state share the same theoretical value of TEE: they have

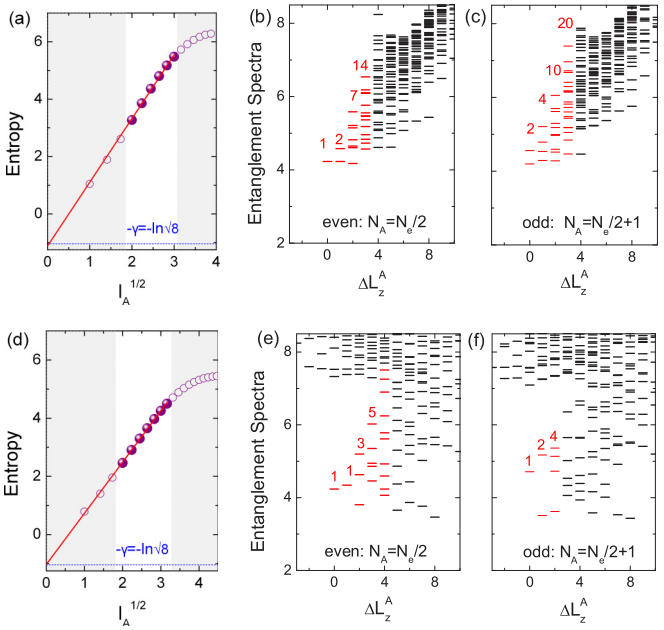

FIG. 3. (a), (d) The entanglement entropy $S(l_A)$ for (a) the (331) Halperin state and (d) the MR Pfaffian state as a function of $\sqrt{l_A}$. The open circles were discarded in the extrapolation because they either represent very small subsystems violating the area law or suffer from the finite-size saturation effect (shaded by gray). The linear extrapolated γ in both cases are in agreement with the predicted value $\ln\sqrt{8}$ (blue dashed line). (b), (c), (e), (f) The low-lying orbital ES of (b), (c) the (331) Halperin state and (e), (f) the MR Pfaffian state, with even or odd electrons in the half-cut subsystem. The countings matching the degeneracy patterns given in the text are labeled by red. All calculations are performed at system size $N_e = 22$ with layer width $w = 1.5$, layer distance $d = 3.0$, and tunneling strengths (a)–(c) $t_\perp = 0.03$ for the (331) state and (d)–(f) $t_\perp = 0.10$ for the MR Pfaffian state.

the same total quantum dimension $\mathcal{D} = \sqrt{8}$, despite hosting different types of quasiparticles [the (331) Halperin state hosts 8 different Abelian quasiparticles, while the MR Pfaffian has 4 Abelian and 2 non-Abelian quasiparticles]. Indeed, both of our extracted results are very close to each other, in agreement with the expectation $\gamma = \ln\sqrt{8} \approx 1.037$ (blue dashed line). Although the definite Abelian or non-Abelian nature cannot be determined by TEE, the observation of a nonzero TEE signals the topologically nontrivial state in the finite-tunneling regime.

B. Orbital entanglement spectrum

The orbital ES, defined as the spectrum of $-\ln\rho_A$, encodes the information of edge excitations [51,52] and has been widely used to identify the emergent FQH phase in a microscopic Hamiltonian [51,53,54]. For various single-layer FQH states, including the Laughlin, Moore-Read [51], and Read-Rezayi states [53,54], the ES has a universal low-energy structure mimicking the pertinent edge excitation spectrum, which is separated from the high-energy nonuniversal part by a finite ES gap. In our bilayer $\nu_T = \frac{1}{2}$ system, different candidates host distinct edge excitations, so we anticipate to distinguish them by the orbital-cut ES. Very recently, the

orbital ES diagnosis was also extended to bilayer $\frac{1}{3}+\frac{1}{3}$ systems [55,56], albeit there is no signal of non-Abelian states in such systems with pure Coulomb interaction (without artificially tuning pseudopotential parameters).

Edge excitations of a specific FQH state are characterized by the degeneracy pattern of the spectrum when plotted versus appropriate quantum numbers, for example, the angular momentum L_z on the sphere. The edge of the (331) Halperin state can be described by two chiral boson fields (Appendix D), thus the corresponding edge excitation spectrum exhibits degeneracy in angular momentum sectors $\Delta L_z = 0,1,2,3,\ldots$ as (Appendix B) [57]

$$\text{even}: 1,2,7,14,\ldots,$$

$$\text{odd}: 2,4,10,20,\ldots,$$

where two sequences are distinguished by the even (odd) number of electrons, and $\Delta L_z = L_z - L_{z,\min}$ with $L_{z,\min}$ the angular momentum where no edge excitations occur. The edge excitations of the MR Pfaffian state, composed of a Majorana fermion mode and a charged-boson mode (Appendix D), should follow the degeneracy pattern (Appendix B) [58]

$$\text{even}: 1,1,3,5,\ldots,$$

$$\text{odd}: 1,2,4,7,\ldots.$$

In contrast, the CFL state does not develop a gapless "edge" spectrum separated from other spectrum by a gap due to its compressible nature.

In Figs. 3(b) and 3(c) and 3(e) and 3(f), we show the DMRG obtained ES for $t_\perp = 0.03$ and 0.10 at layer width $w = 1.5$ and layer distance $d = 3.0$. At weak tunneling $t_\perp = 0.03$, we find that the low-lying ES levels exactly match the degeneracy patterns of the (331) edge spectrum in the first four ΔL_z^A sectors, i.e., 1,2,7,14 for even N_A and 2,4,10,20 for odd N_A, where N_A and ΔL_z^A are the number of electrons and the angular momentum in the subsystem A, respectively. Those low-lying levels are separated from higher ones by a large "entanglement gap." At stronger tunneling $t_\perp = 0.1$, the low-energy ES clearly displays the degeneracy patterns of the MR Pfaffian edge spectrum, i.e., 1,1,3,5 for even N_A and 1,2,4 for odd N_A. Different low-lying ES structures provide compelling evidence that the ground state undergoes a transition from the (331) Halperin phase to the MR Pfaffian phase by tuning $t_\perp$. As shown in Fig. 4(a), with the increase of tunneling $t_\perp$, some ES levels belonging to the (331) Halperin state can be continuously gapped out. After a new entanglement gap Δ_1 is well developed ($t_\perp > 0.05$), the desired ES structure for MR Pfaffian state appears, perfectly matching the prediction that one branch of Majarona fermion mode can be continuously gapped out by the tunneling effect (Appendix D).

IV. QUANTUM PHASE TRANSITION AND PHASE DIAGRAM

To uncover the nature of the quantum phase transition driven by $t_\perp$, we study the evolutions of the ground state and the lowest excited state on the spherical geometry, which have different total angular momenta L_z. We choose fixed layer width $w = 1.5$ and layer distance $d = 3.0$ in these calculations. In Fig. 4(b), we first investigate how the ground-state energy E_0 varies with $t_\perp$. Although E_0 smoothly changes with $t_\perp$, we find a discontinuity in $\partial^2 E_0/\partial^2 t_\perp$ around $t_\perp^{c1} \approx 0.037$. The singularity becomes sharper by increasing the system size, indicating a second-order phase transition in the thermodynamic limit. In Fig. 4(c), we show the excitation gap as a function of $t_\perp$, defined as the energy difference between the first excited state and the ground state [$\Delta_{\text{exc}} = E_1(L_z \neq 0) - E_0(L_z = 0)$]. Δ_{exc} remains finite for all $t_\perp$, consistent with the incompressible nature of the ground state. Interestingly, the excitation gap develops a peak around $t_\perp^{c2} \approx 0.04$. This upward cusp is related to a level crossing between the lowest excited state and higher energy levels [36,37]. These observations lead to two remarks here. First, our calculations support that the transition detected by the ground state and the lowest excited state occurs almost simultaneously ($t_\perp^{c1} \approx t_\perp^{c2}$). Second, our results indicate that the ground state evolves continuously from the (331) Halperin phase to the MR Pfaffian phase, while the excited state with quasihole or quasiparticle excitations changes discontinuously near the phase boundary.

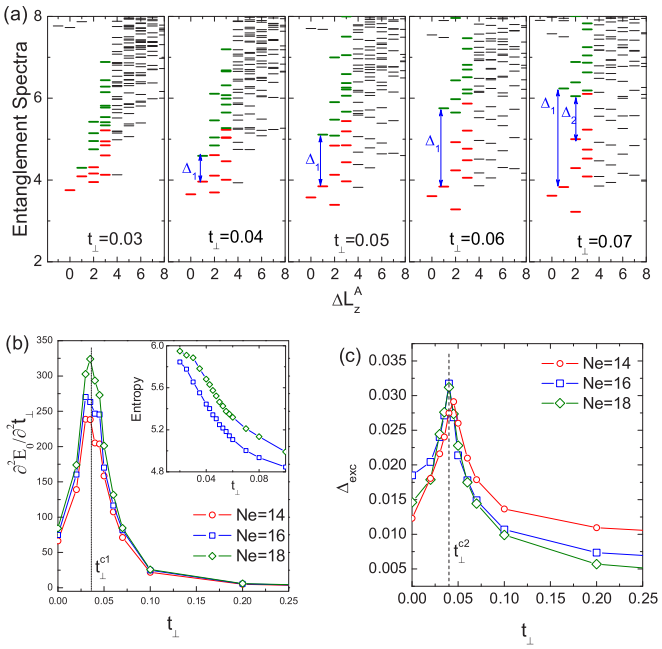

FIG. 4. The continuous phase transition from the (331) Halperin state to the MR Pfaffian state as a function of $t_\perp$ on the sphere. (a) Evolution of ES versus $t_\perp$. The expected levels for the MR Pfaffian state are labeled by red, and redundant levels originally from the (331) Halperin state are labeled by green. $\Delta_{\Delta L_z^A}$ measures the entanglement gap of the MR Pfaffian state in the ΔL_z^A sector. We consider the half-cut subsystem with even number of electrons for $N_e = 18$. (b) Partial derivative $\partial^2 E_0/\partial^2 t_\perp$ as a function of $t_\perp$ for different system sizes $N_e = 14$ (red), 16 (blue), and 18 (green). Inset: evolution of the ground-state entropy with $t_\perp$. (c) The excitation gap Δ_{exc} as a function of $t_\perp$ for various system sizes. All calculations are performed at layer width $w = 1.5$ and layer distance $d = 3.0$.

Compared with the spherical geometry with zero genus where we can only reach one topological sector related to the "highest density profile" (see Appendixes B and D 2), the torus geometry with access to all topological sectors provides

a full picture of the gap closing and the continuous phase transition. As shown in Fig. 2, the energy gap relative to the (331) manifold closes around $t = t_\perp^c$ with one $K = 0$ state in the (331) manifold being continuously gapped out without any level crossing in the low-energy spectrum (also see discussion below). To sum up, our findings provide evidence of the continuous transformation between two triplet pairing states, which was predicted 20 years ago [16,17,24,25].

Intriguingly, the continuous phase transition between the (331) Halperin state and the MR Pfaffian state can be understood [16] from several perspectives. In Appendix D, in addition to the wave-function equivalence, we propose two independent perspectives to understand the transition in the bulk and on the edge, respectively. First, by the perturbation theory, we construct a low-energy effective model, which clearly shows that, at least in the thin-torus limit [30,47], the system can indeed undergo a continuous phase transition (with the same critical behavior as the transverse field Ising model [59]) when the tunneling $t_\perp$ increases, and one state in the ground-state manifold is gapped out, thus changing the ground-state degeneracy from the (331) type to the MR Pfaffian type. We believe this conclusion is still true when the system adiabatically deforms from the thin-torus limit to the square torus. Second, starting from the edge theory of the (331) Halperin state described by two chiral bosons (with total central charge $c = 2$) [60,61], we find that the interlayer tunneling tends to produce a Majorana neutral mode carrying $c = \frac{1}{2}$ in addition to the usual $c = 1$ bosonic charge mode [29,62], thus reaching the edge theory of the MR Pfaffian state. Therefore, from the viewpoints of the wave-function equivalence, the bulk theory in the thin-torus limit, and the effective edge theory, a continuous phase transition is allowed between these two triplet pairing FQH states [17,25].

At last, we present a quantum phase diagram for the FQH bilayer system at $\nu_T = \frac{1}{2}$, as functions of experimentally relevant parameters d and $t_\perp$ in Fig. 5. Different phases and

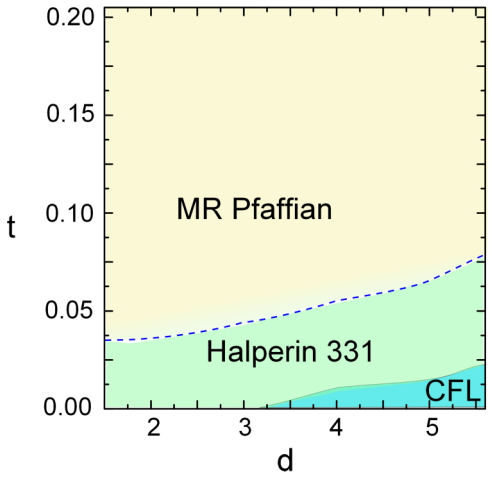

FIG. 5. The phase diagram of the FQH bilayer at $\nu_T = \frac{1}{2}$ in terms of the layer distance d and tunneling strength $t_\perp$, obtained from $N_e = 18$ on the sphere with layer width $w = 1.5$. The continuous phase transition from the (331) Halperin state to the MR Pfaffian state is labeled by dashed line, while the solid line marks the transition between the (331) Halperin state and a possible CFL.

their phase boundaries are determined by the entanglement spectrum based on the $N_e = 18$ data on the sphere. We find three different phases: the (331) Halperin phase, the MR Pfaffian phase, and the compressible CFL phase. When $t_\perp$ is small and d is relatively large, two layers are effectively decoupled with each at $\nu = \frac{1}{4}$ (in the $d \to \infty$ limit) and the ground state is a well-known CFL. At small $t_\perp$, the ground state is in the (331) Halperin phase, then a phase transition to the MR Pfaffian state occurs at $t_\perp \sim 0.04$–0.07 (depending on the value of d). The intermediate tunneling regime $t_\perp \sim 0.05$–0.1 has larger excitation gap as shown in Fig. 4(c), where the MR Pfaffian state is most likely to be observed experimentally (Appendix F). Interestingly, the maximal excitation gap in the intermediate-tunneling regime [Fig. 4(c)] qualitatively agrees with the experimental observation [21]. This also supports that MR Pfaffian state is more robust in the intermediate-tunneling regime while the (331) Halperin state is stable in the weak-tunneling regime. In addition, we point out that, even though the MR Pfaffian phase is shown to be remarkably robust in the intermediate-tunneling regime, we are less certain about the fate of the state in the strong-tunneling limit ($t_\perp \to \infty$) (see Appendix E 2) due to other competing phases.

V. CONCLUSION

In this work, we use density-matrix renormalization group and exact diagonalization techniques to study a fractional quantum Hall (FQH) bilayer system at total half filling. In the phase diagram in terms of the experimentally accessible parameters (layer separation d, interlayer tunneling $t_\perp$, and layer width w), we find two different incompressible phases: the Abelian (331) Halperin phase in the weak-tunneling regime and the non-Abelian Moore-Read (MR) Pfaffian state for the intermediate-tunneling strength, as identified by the ground-state degeneracy on the torus geometry and the topological entanglement-based diagnosis on the spherical geometry. The results on different geometries are consistent with each other and give similar phase boundaries. We also establish that the transition between these two phases is continuous, which verifies the theoretical conjecture that a continuous phase transition is allowed between two triplet pairing states [17,25] with distinct quasiparticle excitations. Our work clearly demonstrates that for realistic two-component FQH systems, the non-Abelian MR Pfaffian state is indeed a stronger candidate than the Abelian (331) Halperin state in the intermediate-tunneling regime.

We believe that our work will motivate experimental activities searching for the non-Abelian phase in bilayer structures at total half filling. Some existing theoretical proposals can be used to identify the corresponding edge physics experimentally [52,63,64]. For example, the quasiparticle tunneling conductance crossing quantum point contacts allows the extraction of the dimensionless interaction parameter g, which reflects the topological order in the bulk and can be directly compared with the theoretical expectations of $g = \frac{1}{4}$ for the MR Pfaffian state and $g = \frac{3}{8}$ for the (331) Halperin state [10,13]. Another approach is to probe the edge density fluctuation when the sample is coupled to a nearby quantum dot [64]. Furthermore, the measurement of drag Hall conductance in double QWs can be performed to identify different phases. The (331)

Halperin state has the quantized Hall drag conductance, while the MR Pfaffian state has a strong density fluctuation with nonquantized Hall drag conductance (see Appendix F). On the theoretical sides, our work, with combined DMRG and ED methods, also paves the way for future studies of other multicomponent systems with the aim to search for more exotic FQH states.

Note added. Recently, we noticed experimental evidences of an incompressible one-component state at $\nu = \frac{1}{2}$ [65,66].

ACKNOWLEDGMENTS

W.Z. thanks Z.-X. Hu, M. Peterson, C. J. Wang, and T. S. Zeng for fruitful discussion, and L. Wang for preparing Fig. 1. We also thank N. Regnault and Z. Papic for useful comments and X. G. Wen for stimulating discussion. This work is supported by the US Department of Energy, Office of Basic Energy Sciences under Grants No. DE-FG02-06ER46305 (W.Z. and D.N.S.) and No. DE-SC0002140 (F.D.M.H. and Z.L.), the latter also for the use of computational facilities at Princeton University. Z.L. was additionally supported by Alexander von Humboldt Research Fellowship for Postdoctoral Researchers. F.D.M.H. also acknowledges partial support from the W. M. Keck Foundation. We also acknowledge travel funding support from the Princeton Center for Complex Materials, a MRSEC supported by NSF Grant No. DMR 1420541.

APPENDIX A: COMPUTATIONAL METHODS

1. Fractional quantum Hall bilayer Hamiltonian

In a perpendicular external magnetic field, electrons moving in two spatial dimensions occupy highly degenerate orbitals in each Landau level. When the magnetic field is strong, we can assume that electrons are spin polarized (in experiments, the Zeeman energy is order of Kelvin, which is indeed much larger than the reported energy gap) and their dynamics is restricted to the orbitals in the lowest Landau level (LLL). Under these circumstances, the Hamiltonian of a fractional quantum Hall (FQH) bilayer system can be written as

$$\begin{aligned} H = & \sum_{\{m_i\}=0}^{N_s-1} \sum_{\sigma=\uparrow,\downarrow} V^{\sigma\sigma}_{m_1,m_2,m_3,m_4} c^\dagger_{m_1\sigma} c^\dagger_{m_2\sigma} c_{m_3\sigma} c_{m_4\sigma} \\ & + \sum_{\{m_i\}=0}^{N_s-1} \sum_{\sigma=\uparrow,\downarrow} V^{\sigma\bar{\sigma}}_{m_1,m_2,m_3,m_4} c^\dagger_{m_1\sigma} c^\dagger_{m_2\bar{\sigma}} c_{m_3\bar{\sigma}} c_{m_4\sigma} \\ & - t_\perp \sum_{m=0}^{N_s-1} \sum_{\sigma=\uparrow,\downarrow} c^\dagger_{m,\sigma} c_{m,\bar{\sigma}}, \end{aligned} \tag{A1}$$

where N_s is the total number of LLL orbitals in each layer, $c^\dagger_{m,\sigma}$ ($c_{m,\sigma}$) is the creation (annihilation) operator of an electron in the LLL orbital m of layer $\sigma(\bar{\sigma}) = \uparrow(\downarrow), \downarrow(\uparrow)$, and $t_\perp$ describes the tunneling strength between two layers. $V^{\sigma\sigma}_{m_1,m_2,m_3,m_4}$ and $V^{\sigma\bar{\sigma}}_{m_1,m_2,m_3,m_4}$ are matrix elements of the intralayer and interlayer interaction, respectively, which can be computed by the standard second-quantization procedure once we adopt a specific geometry for the system. In the following, we give the details on the torus geometry and spherical geometry that we use in the main text.

2. Torus geometry

The advantage of the torus geometry is its nonzero genus, which allows us to distinguish different topological orders by their ground-state degeneracies. We consider N_e electrons moving on two rectangular tori with a perpendicular magnetic field. Each torus, corresponding to a layer, is spanned by $\mathbf{L}_1 = L_1\mathbf{e}_x$ and $\mathbf{L}_2 = L_2\mathbf{e}_y$, where $\mathbf{e}_x$ and $\mathbf{e}_y$ are fixed Cartesian unit vectors, and L_1 and L_2 are lengths of the two fundamental cycles of the torus. Required by the magnetic translation invariance, the number of fluxes N_ϕ penetrating each torus, which is equal to the number of orbitals N_s in one Landau level per layer, must be an integer $N_s = N_\phi = L_1L_2/(2\pi\ell^2)$. The total filling fraction in two layers is then defined as $\nu_T = N_e/N_\phi = N_e/N_s$. In the following, we set the magnetic length $\ell = 1$ as the length unit. In the Landau gauge $\mathbf{A} = Bx\mathbf{e}_y$, the basis of LLL single-particle states can be taken as $\psi^\sigma_j(x_\sigma, y_\sigma) = (\frac{1}{\sqrt{\pi}L_2})^{\frac{1}{2}} \sum_{n=-\infty}^{+\infty} e^{\mathrm{i}\frac{2\pi}{L_2}(j+nN_s)y_\sigma} e^{-\frac{1}{2}[x_\sigma - \frac{2\pi}{L_2}(j+nN_s)]^2}$, where (x_σ, y_σ) is the coordinate in layer σ and $j = 0,1,\ldots,N_s-1$ is the orbital momentum. Then, the standard second-quantization procedures give

$$\begin{aligned} V^{\sigma\sigma'}_{m_1,m_2,m_3,m_4} = & \delta^{\mathrm{mod}N_s}_{m_1+m_2,m_3+m_4} \frac{1}{4\pi N_s} \\ & \times \sum_{q_1,q_2=-\infty}^{+\infty} \delta^{\mathrm{mod}N_s}_{q_2,m_1-m_4} V_{\sigma\sigma'}(q_x,q_y) \\ & \times e^{-\frac{1}{2}(q_x^2+q_y^2)} e^{\mathrm{i}\frac{2\pi q_1}{N_s}(m_1-m_3)}, \end{aligned} \tag{A2}$$

where $q_x = \frac{2\pi q_1}{L_1}$, $q_y = \frac{2\pi q_2}{L_2}$, and $V^{\sigma\sigma'}(\mathbf{q})$ is the Fourier transform of the interaction in real space.

The detailed form of $V_{\sigma\sigma'}(\mathbf{q})$ depends on the theoretical model of our bilayer FQH system. In this work, we consider Coulomb-interacting electrons in double quantum wells, each of which is described by an infinite square well with width w and separated from each other by distance d. Then, we have

$$V_{\sigma\sigma}(\mathbf{q}) = \frac{1}{q} \frac{3qw + \frac{8\pi^2}{qw} - \frac{32\pi^4(1-e^{-qw})}{q^2w^2(q^2w^2+4\pi^2)}}{q^2w^2+4\pi^2} \tag{A3}$$

for the intralayer interaction, and

$$V_{\sigma\bar{\sigma}}(\mathbf{q}) = \frac{1}{q} e^{-qd} \tag{A4}$$

for the interlayer interaction. For simplicity, we ignore the nonzero layer width in the interlayer interaction. The nonzero layer width just quantitatively modifies the effective layer distance, which should not change intrinsic physics shown in the main text. For physical setting, we force the condition $d > w$ in the calculations. These choices can well describe the experimental setups in GaAs/AlAs systems.

The magnetic translation invariance in two directions on the torus geometry allows us to label each many-body eigenstate of the Hamiltonian (A1) by a two-dimensional momentum (K_1, K_2). In our exact diagonalization calculation, we utilize the full symmetry (K_1, K_2). However, in the DMRG calculation, we only use one quantum number K_2 (relabeled as K), which is the total orbital momentum of the system.

3. Spherical geometry

Compared with the torus geometry, spherical geometry has zero genus, thus we cannot distinguish different topological orders by their ground-state degeneracies. However, the unique ground state and a single edge per layer for the orbital cut liberate us from the complicated ground-state superposition and edge mode combination that may happen on the torus, thus making the spherical geometry a particularly suitable platform for the entanglement spectroscopy.

We use Haldane's representation of the spherical geometry [67]. In our bilayer FQH system, N_e electrons are confined on the surfaces of two spheres. Each sphere, corresponding to a layer, contains a magnetic monopole of strength Q. The total number of magnetic fluxes through each spherical surface is quantized to be an integer $N_\phi = 2Q$. The basis of LLL single-particle states can be taken as $\psi_j^\sigma(u_\sigma, v_\sigma) = \sqrt{\frac{(2Q+1)!}{4\pi(Q+j)!(Q-j)!}} u_\sigma^{Q+j} v_\sigma^{Q-j}$ with orbital angular momentum $j = -Q, -Q+1, \ldots, Q$, thus there are $N_s = N_\phi + 1 = 2Q+1$ orbitals in the LLL. (u_σ, v_σ) is the spinor variable in layer σ with $u = \cos(\theta/2)e^{i\phi/2}$ and $v = \sin(\theta/2)e^{-i\phi/2}$, where θ and ϕ are the spherical coordinates. The total filling fraction in two layers is defined as $\nu_T = N_e/(N_\phi + \mathcal{S}) = N_e/(N_s + \mathcal{S} - 1)$, where $\mathcal{S}$ is a finite-size shift on sphere. Please note that both the (331) Halperin state and Moore-Read Pfaffian state live in $\mathcal{S} = 3$. Standard second-quantization procedures lead to

$$V^{\sigma\sigma'}_{m_1,m_2,m_3,m_4} = \delta_{m_1+m_2,m_3+m_4} \frac{1}{2} \sum_{l=0}^{2Q} \mathcal{V}_l^{\sigma\sigma'} [2(2Q-l)+1] \times \begin{pmatrix} Q & Q & 2Q-l \\ m_1-Q & m_2-Q & 2Q-(m_1+m_2) \end{pmatrix} \times \begin{pmatrix} Q & Q & 2Q-l \\ m_4-Q & m_3-Q & 2Q-(m_3+m_4) \end{pmatrix}, \tag{A5}$$

where $m_{1,2,3,4} = 0, 1, \ldots, 2Q$, $\begin{pmatrix} \cdot & \cdot & \cdot \\ \cdot & \cdot & \cdot \end{pmatrix}$ is the Wigner $3-j$ symbol, and $\mathcal{V}_l^{\sigma\sigma'}$ is the Haldane's pseudopotential parameter of the interaction. For simplicity, we just use the LLL pseudopotential parameters on an infinite plane obtained by

$$\mathcal{V}_l^{\sigma\sigma'} = \frac{1}{(2\pi)^2} \int V_{\sigma\sigma'}(\mathbf{q}) \mathcal{L}_l(q^2) e^{-q^2} d^2\mathbf{q}, \tag{A6}$$

where $\mathcal{L}_l$ is the Laguerre polynomial, and $V_{\sigma\sigma'}(\mathbf{q})$ is given by Eqs. (A3) and (A4).

The symmetry that we use in our calculation is the conservation of the total orbital angular momentum L_z on the sphere.

4. Density-matrix renormalization group

In the main text, our calculations are based on the unbiased density-matrix renormalization group (DMRG) algorithm [41–44]. The technical details about DMRG in momentum space have been reported in our previous studies [44]. There, it has been shown that, for the single-layer $\nu = \frac{1}{3}$ Laughlin state and the $\nu = \frac{5}{2}$ Moore-Read Pfaffian state, DMRG can get reliable results with very high accuracy in much larger systems than the limit of exact diagonalization. Now, we find that DMRG also has excellent performance in our bilayer FQH system on the torus and spherical geometry. We have obtained the ground state for the spherical (toroidal) system up to $N_e = 24$ ($N_e = 12$) electrons by keeping up to 12 000 states, which leads to a truncation error smaller than 3×10^{-5} in the final sweep. We also emphasize that, for the calculations on the torus geometry, since we need to track two ground states in each momentum sector simultaneously, the fully converged results are limited to $N_e = 12$. Compared with the torus geometry, the calculations on the spherical geometry can reach systems as large as $N_e = 24$ within controlled accuracy.

APPENDIX B: COUNTING OF EDGE EXCITATIONS

1. Moore-Read Pfaffian state

Here, we analyze the degeneracy pattern of the edge excitation spectrum of the fermionic Moore-Read (MR) Pfaffian state. Our analysis is based on root configurations [68] on the sphere, which are also equivalent to configurations in the thin-torus limit [69,70]. The degeneracy of the MR Pfaffian edge excitations is the same as the number of root configurations that satisfy a specific generalized exclusion rule, i.e., no more than 2 fermions in 4 consecutive orbitals.

In Tables I and II, we count the root configurations that satisfy this rule. We start from the initial root configuration without edge excitations, for example, 1100110011|0000, which is just the root configuration of the MR Pfaffian state itself. "...|..." indicates the right edge, which is open so electrons can hop across to form edge excitations. The root configurations with edge excitations must have larger angular momentum L_z than the initial one. We list all of them in terms of their relative angular momentum ΔL_z to the initial root configuration, for which $\Delta L_z = 0$. Note that root configurations and their counting are different for even number (Table I) and odd number (Table II) of electrons.

TABLE I. In this table, we count the root configurations of the MR Pfaffian edge excitations with even N_e. The counting is $1,1,3,5,\ldots$ in the $\Delta L_z = 0,1,2,3,\ldots$ sector.

$\Delta L_z = 0$	$\Delta L_z = 1$	$\Delta L_z = 2$	$\Delta L_z = 3$
1100110011|0000	1100110010|1000	1100110010|0100	1100110010|0010
		1100110001|1000	1100110001|0100
		1100101010|1000	1100101010|0100
			1100101001|1000
			1010101010|1000

TABLE II. In this table, we count the root configurations of the MR Pfaffian edge excitations with odd N_e. The counting is 1,2,4,7, ... in the $\Delta L_z = 0,1,2,3, \ldots$ sector.

$\Delta L_z = 0$	$\Delta L_z = 1$	$\Delta L_z = 2$	$\Delta L_z = 3$
110011001|0000	110011000|1000	110011000|0100	110011000|0010
	110010101|0000	110010100|1000	110010100|0100
		110010011|0000	110010010|1000
		101010101|0000	110001100|1000
			101010100|1000
			101010011|0000
			1010101010101|0000

The counting of edge excitations given above is saturated only in the thermodynamic limit. In finite systems, we can only observe part of them. For example, in Table II, the root configuration 1010101010101|0000 in the $\Delta L_z = 3$ sector requires at least 7 electrons in the system. So, this excitation cannot be observed in smaller system sizes.

We can also count the edge excitation modes from the effective edge Hamiltonian. The edge excitation of the MR Pfaffian state contains one branch of free bosons and one branch of Majorana fermions (also see Appendix D 2) with either periodic or antiperiodic boundary conditions. For free bosons plus antiperiodic Majorana fermions (which corresponds to the ground state on the sphere), the excitation spectrum is described by the Hamiltonian [58,71]

$$H_{\text{edge}}^{\text{AP}} = \sum_{m>0} [E_b(m) b_m^\dagger b_m + E_f(m-1/2) c_{m-1/2}^\dagger c_{m-1/2}], \tag{B1}$$

where b and $b^\dagger$ (c and $c^\dagger$) are standard boson (fermion) creation and annihilation operators, $E_b(m)$ [$E_f(m)$] is the dispersion relation of bosons (fermions) and the total momentum operator is defined as $K = \sum_{m>0} [m b_m^\dagger b_m + (m - 1/2) c_{m-1/2}^\dagger c_{m-1/2}]$. The degeneracy of the edge excitations is the same as the number of energy levels in each K sector, and depends on the parity of the number of fermions $(-1)^F$, $F = \sum_{m>0} c_{m-1/2}^\dagger c_{m-1/2}$. For even F, the counting is 1,1,3,5,10, ... at $\Delta K = 0,1,2,3,4, \ldots$; while for odd F, the counting is 1,2,4,7,13, ... at $\Delta K = 0,1,2,3,4, \ldots$. Here, ΔK is defined as $K - K_0$ where K_0 is the lowest momentum ($K_0 = 0$ for even F and $K_0 = \frac{1}{2}$ for odd F). One can see that this method reaches exactly the same counting as that obtained by root configurations.

2. (331) Halperin state

In bilayer FQH systems, it is convenient to consider the orbital m in the upper layer and the orbital m in the lower layer as a site with four possible occupations: 0 (no electrons), $\uparrow$ (one electron in the upper layer), $\downarrow$ (one electron in the lower layer), and 2 (two electrons, one in each layer). In this site basis, the root configuration of the (331) state on the sphere is $XX00XX00 \ldots XX00XX$ [30], where $XX \equiv (\uparrow\downarrow + \downarrow\uparrow)/\sqrt{2}$ is the triplet between two nearest-neighbor sites. The root configurations of the (331) state and its edge excitations obey the following generalized exclusion rule: (1) there is no more than one electron in three consecutive orbitals within each layer; (2) the configuration of 2 is forbidden; (3) electrons on two nearest neighbor sites must form the triplet XX. Some configurations, for example $XX02, XX0XX, XX\uparrow, XX\downarrow, XX0\uparrow, XX0\downarrow, \uparrow\uparrow, \uparrow 0\uparrow, \downarrow\downarrow, \downarrow 0\downarrow$ violate this generalized exclusion rule, thus they cannot appear in the root configurations. With this generalized exclusion rule, we can count the root

TABLE III. In this table, we count the root configurations of the (331) edge excitations with even N_e. The counting is 1,2,7,14, ... in the $\Delta L_z = 0,1,2,3, \ldots$ sector. We also give the pseudospin quantum number $S_z = (N_e^\uparrow - N_e^\downarrow)/2$ for each root configuration.

$\Delta L_z = 0$	$\Delta L_z = 1$	$\Delta L_z = 2$	$\Delta L_z = 3$
$XX00XX00XX\|000$ ($S_z = 0$)	$XX00XX00 \uparrow 0\| \downarrow 00$ ($S_z = 0$)	$XX00XX00 \uparrow 0\|0 \downarrow 0$ ($S_z = 0$)	$XX00XX00 \uparrow 0\|00 \downarrow$ ($S_z = 0$)
	$XX00XX00 \downarrow 0\| \uparrow 00$ ($S_z = 0$)	$XX00XX00 \downarrow 0\|0 \uparrow 0$ ($S_z = 0$)	$XX00XX00 \downarrow 0\|00 \uparrow$ ($S_z = 0$)
		$XX00XX000X\|X00$ ($S_z = 0$)	$XX00XX000 \uparrow \|0 \downarrow 0$ ($S_z = 0$)
		$XX00 \uparrow 0 \downarrow 0 \uparrow 0\| \downarrow 00$ ($S_z = 0$)	$XX00XX000 \downarrow \|0 \uparrow 0$ ($S_z = 0$)
		$XX00 \downarrow 0 \uparrow 0 \downarrow 0\| \uparrow 00$ ($S_z = 0$)	$XX00 \uparrow 0 \downarrow 0 \uparrow 0\|0 \downarrow 0$ ($S_z = 0$)
		$XX00XX00 \uparrow 0\|0 \uparrow 0$ ($S_z = 1$)	$XX00 \downarrow 0 \uparrow 0 \downarrow 0\|0 \uparrow 0$ ($S_z = 0$)
		$XX00XX00 \downarrow 0\|0 \downarrow 0$ ($S_z = -1$)	$XX00 \uparrow 0 \downarrow 00X\|X00$ ($S_z = 0$)
			$XX00 \downarrow 0 \uparrow 00X\|X00$ ($S_z = 0$)
			$\uparrow 0 \downarrow 0 \uparrow 0 \downarrow 0 \uparrow 0\| \downarrow 00$ ($S_z = 0$)
			$\downarrow 0 \uparrow 0 \downarrow 0 \uparrow 0 \downarrow 0\| \uparrow 00$ ($S_z = 0$)
			$XX00XX00 \uparrow 0\|00 \uparrow$ ($S_z = 1$)
			$XX00 \uparrow 0 \downarrow 0 \uparrow 0\|0 \uparrow 0$ ($S_z = 1$)
			$XX00XX00 \downarrow 0\|00 \downarrow$ ($S_z = -1$)
			$XX00 \downarrow 0 \uparrow 0 \downarrow 0\|0 \downarrow 0$ ($S_z = -1$)

TABLE IV. In this table, we count the root configurations of the (331) edge excitations with odd N_e. The counting is 2,4,10, ... in the $\Delta L_z = 0,1,2,\ldots$ sector. We also give the pseudospin quantum number $S_z = (N_e^{\uparrow} - N_e^{\downarrow})/2$ for each root configuration.

$\Delta L_z = 0$	$\Delta L_z = 1$	$\Delta L_z = 2$
$XX00XX00 \uparrow \vert 000$ $(S_z = 1/2)$	$XX00XX000\vert \uparrow 00$ $(S_z = 1/2)$	$XX00XX000\vert 0 \uparrow 0$ $(S_z = 1/2)$
$XX00XX00 \downarrow \vert 000$ $(S_z = -1/2)$	$XX00 \uparrow 0 \downarrow 0 \uparrow \vert 000$ $(S_z = 1/2)$	$XX00 \uparrow 0 \downarrow 00\vert \uparrow 00$ $(S_z = 1/2)$
	$XX00XX000\vert \downarrow 00$ $(S_z = -1/2)$	$XX00 \downarrow 0 \uparrow 00\vert \uparrow 00$ $(S_z = 1/2)$
	$XX00 \downarrow 0 \uparrow 0 \downarrow \vert 000$ $(S_z = -1/2)$	$XX00 \uparrow 00XX\vert 000$ $(S_z = 1/2)$
		$\uparrow 0 \downarrow 0 \uparrow 0 \downarrow 0 \uparrow \vert 000$ $(S_z = 1/2)$
		$XX00XX000\vert 0 \downarrow 0$ $(S_z = -1/2)$
		$XX00 \uparrow 0 \downarrow 00\vert \downarrow 00$ $(S_z = -1/2)$
		$XX00 \downarrow 0 \uparrow 00\vert \downarrow 00$ $(S_z = -1/2)$
		$XX00 \downarrow 00XX\vert 000$ $(S_z = -1/2)$
		$\downarrow 0 \uparrow 0 \downarrow 0 \uparrow 0 \downarrow \vert 000$ $(S_z = -1/2)$

configurations of the (331) edge excitations, as shown in Tables III and IV. Again, the root configurations and their counting are different for even number (Table III) and odd number (Table IV) of electrons.

APPENDIX C: ADDITIONAL RESULTS OF ENTANGLEMENT SPECTRA

An artificial edge is produced by the orbital cut of the whole system into two parts. The low-lying entanglement spectrum (ES) mimics the edge excitation spectrum of one subsystem across the cutting edge. Thus, the counting structure in the ES can be predicted by applying the analysis in Appendix B to that subsystem, whose initial root configuration is the corresponding subsystem part of the root configuration of the whole system. Here, we show the ground-state orbital ES in the MR Pfaffian phase of our bilayer FQH system for various system sizes $N_e = 16$, 18, 20, 22, and 24 (Fig. 6). One can see that the leading ES counting at all system sizes always displays 1,1,3 (1,2,4) for even (odd) number of electrons in the half-cut subsystem, matching the predictions in Tables I and II. For $N_e = 20$, we observe a relatively small entanglement gap, which might be attributed to that this system size is "aliased" to another possible FQH state at $\nu = \frac{4}{7}$ on the sphere. If we go to larger systems like $N_e = 22$ and 24, the entanglement gap becomes stronger again. Here, the low-lying ES structure is robust against finite-size effect, providing a fingerprint of the non-Abelian MR Pfaffian nature of the ground state.

We also track the evolution of the ground-state orbital ES as a function of the tunneling strength $t_\perp$. In Fig. 7, we show the ES by varying $t_\perp$ from 0.02 to 0.10 at layer width $w = 1.5$ and layer distance $d = 3.0$. In the weak-tunneling regime ($t_\perp < 0.04$), the leading ES counting matches the expectation of the (331) Halperin state in Tables III and IV. Remarkably, with increasing $t_\perp$, some levels in angular momentum sectors $\Delta L_z^A \geqslant 1$ are being continuously gapped out. For example, at $t_\perp = 0.05$, the gap between the lowest level and the second lowest level in the $\Delta L_z^A = 1$ sector becomes visible, indicating the MR Pfaffian ES is developing. The fact that some edge modes in the ES of the (331) Halperin state are continuously being gapped out with increasing the tunneling strength $t_\perp$ is consistent with the effective edge theory described in Appendix D 2.

APPENDIX D: THEORETICAL CONSIDERATION

In this appendix, we review several different theories to understand the relation between the non-Abelian MR Pfaffian state and the Abelian (331) Halperin state. First, with the help of Cauchy identity, we show that the antisymmetrized (331) Halperin wave function leads to the MR Pfaffian wave function. Second, by including the tunneling effect, it is plausible to reach the edge theory of the MR Pfaffian state from that of the (331) Halperin state via gapping out one branch of Majorana fermion from the neutral mode. Third, working in the thin-torus limit, the quantum phase transition from the (331) Halperin state to the MR Pfaffian state can be captured by an effective one-dimensional transverse-field Ising model, which helps us to elucidate the nature of the transition.

1. Model wave function

It has been a long time since the discovery of the exact equivalence [24,25] between the MR Pfaffian wave function [4] and the antisymmetrized (331) Halperin wave function [14]. Specifically, the MR Pfaffian wave function can be written as (we discard the Gaussian exponential factor hereafter)

$$\Psi_{\mathrm{MR}} = \prod_{i<j}(z_i - z_j)^2 \mathrm{Pf}\left(\frac{1}{z_i - z_j}\right), \tag{D1}$$

where z_i's are two-dimensional coordinates of electrons, and $\mathrm{Pf}(M_{ij}) = \mathcal{A}(M_{12}M_{34}\ldots M_{N-1,N})$ with $\mathcal{A}$ the antisymmetrization operator. The (331) Halperin wave function is

$$\Psi_{331} = \prod_{i<j}(z_i^{\uparrow} - z_j^{\uparrow})^3 \prod_{k<l}(w_k^{\downarrow} - w_l^{\downarrow})^3 \prod_{m,n}(z_m^{\uparrow} - w_n^{\downarrow}), \tag{D2}$$

where $z_i^{\uparrow}$'s and $w_i^{\downarrow}$'s are coordinates of electrons in the top and bottom layers denoted by the pseudospin indices $\uparrow$ and $\downarrow$, respectively. It is important to note that the (331) Halperin wave function can be analytically cast in to a paired form

$$\Psi_{331} = \prod_{i<j}(x_i - x_j)^2 \det\left[\frac{1}{z_i^{\uparrow} - w_j^{\downarrow}}\right]$$

with the help of the Cauchy identity [24] $\frac{\prod_{i<j}(z_i^{\uparrow} - z_j^{\uparrow})\prod_{k<l}(w_k^{\downarrow} - w_l^{\downarrow})}{\prod_{m,n}(z_m^{\uparrow} - w_n^{\downarrow})} = \det[\frac{1}{z_i^{\uparrow} - w_j^{\downarrow}}]$, where $\{x_i\}$ includes

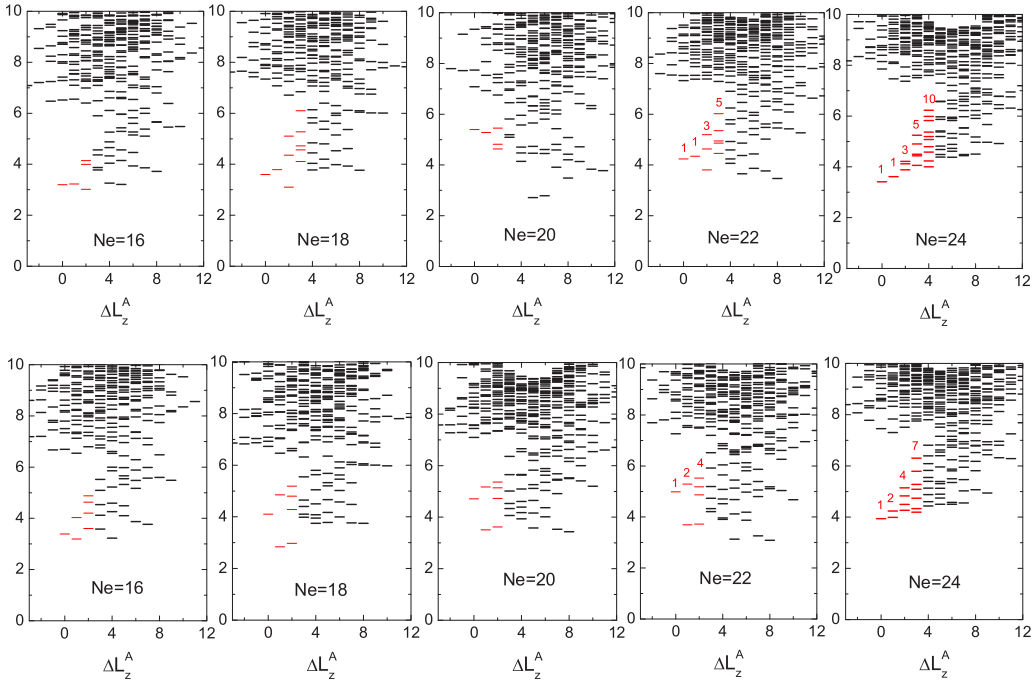

FIG. 6. The low-lying orbital ES for various bilayer system sizes $N_e = 16,18,20,22,24$ at the tunneling strength $t_\perp = 0.10$, layer width $w = 1.5$, and layer distance $d = 3.0$, with even (top) or odd (bottom) number of electrons in the half-cut subsystem. The levels whose counting is consistent with the MR Pfaffian edge excitations proposed in Tables I and II are labeled by red. $\Delta L_z^A = L_z^A - L_{z,\min}^A$, where $L_{z,\min}^A$ is the total angular momentum of the subsystem A without edge excitations.

all $z_i^\uparrow$'s and $w_i^\downarrow$'s. Then, a further antisymmetrization precisely produces the MR Pfaffian wave function (up to a constant normalization factor), leading to

$$\Psi_{\rm MR} = \mathcal{A}\Psi_{331}. \tag{D3}$$

2. Effective edge theory

Another efficient way to investigate the possible transition between the (331) Halperin state and the MR Pfaffian state is the effective edge theory. The key idea is that, starting from the (331) edge theory described by two chiral boson fields [central charge $c = 2$ in conformal field theory (CFT)], the tunneling effect between two layers tends to replace one boson field by a Majorana fermion field carrying $c = \frac{1}{2}$, while the other $c = 1$ boson field is remained.

More precisely, we start from the edge theory of the (331) Halperin state. The gapless excitations are confined to two edges of the droplet, described by the action [61]

$$S_{\rm edge} = \frac{1}{4\pi}\int dt\, dx [K_{IJ}\partial_t u_I \partial_x u_J - V_{IJ}\partial_x u_I \partial_x u_J]$$

and the Hamiltonian

$$H_{\rm edge} = \frac{1}{4\pi}\int dt\, dx\, V_{IJ}\partial_x u_I \partial_x u_J. \tag{D4}$$

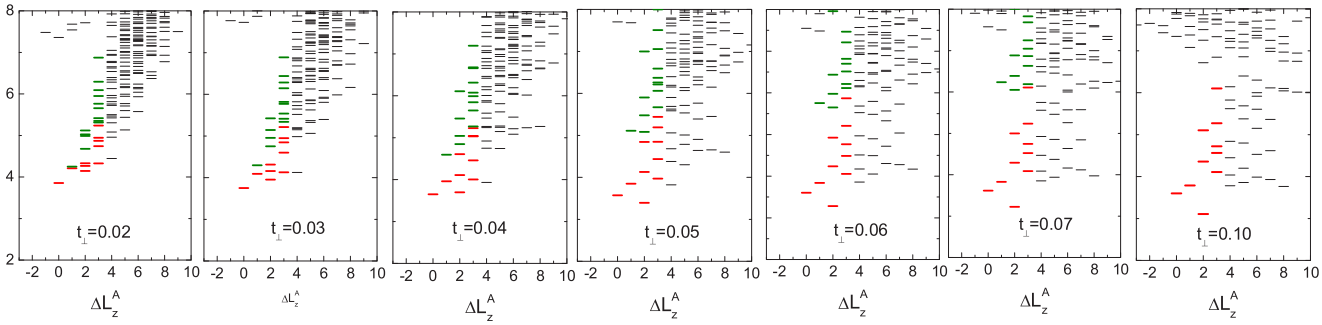

FIG. 7. The low-lying orbital ES of $N_e = 18$ for different tunneling strength $t_\perp$ at layer width $w = 1.5$ and layer distance $d = 3.0$, with even number of electrons in the half-cut subsystem. The levels whose counting is consistent with the MR Pfaffian edge excitations proposed in Tables I and II are labeled by red. The green levels match the (331) edge excitations proposed in Tables III and IV at small $t_\perp$, but are continuously gapped out with increasing the tunneling strength. $\Delta L_z^A = L_z^A - L_{z,\min}^A$, where $L_{z,\min}^A$ is the total angular momentum of the subsystem A without edge excitations.

The matrix K_{IJ} which characterizes the topological properties of the (331) Halperin state has the form of

$$K = \begin{pmatrix} 3 & 1 \\ 1 & 3 \end{pmatrix}. \tag{D5}$$

$u_I(t,x)$ ($I = 1,2$ corresponding to two layers) are chiral bosonic fields describing two edge currents along the x direction, which satisfy the equal-time commutation relation

$$[u_I(t,x),u_J(t,x')] = i\pi K_{IJ}\,\mathrm{sgn}(x-x'). \tag{D6}$$

The matrix V_{IJ} which contains the information of interactions between the edges has the form of

$$V = \begin{pmatrix} v & g \\ g & v \end{pmatrix}, \tag{D7}$$

where we require $g^2 < v^2$ so V is positive definite.

H_{edge} in Eq. (D4) can be simplified by an orthogonal transformation on the chiral bosonic fields

$$\begin{pmatrix} u_1 \\ u_2 \end{pmatrix} = \begin{pmatrix} \sqrt{2} & -1 \\ \sqrt{2} & 1 \end{pmatrix} \begin{pmatrix} \phi_c \\ \phi_n \end{pmatrix}, \tag{D8}$$

leading to

$$H_{\mathrm{edge}} = \frac{1}{4\pi}\int dt\,dx[v_c(\partial_x\phi_c)^2 + v_n(\partial_x\phi_n)^2]. \tag{D9}$$

We refer to the new bosonic fields ϕ_c and ϕ_n as the charged and neutral edge mode, respectively [29,62]. ϕ_c is related to the total electric charge on the two edges with velocity $v_c = 4(v+g)$, while ϕ_n is related to the difference between two edges with velocity $v_n = 2(v-g)$. In terms of the new fields, the commutators are now independent:

$$\begin{aligned}[\phi_c(t,x),\phi_c(t,x')] &= i\pi\ \mathrm{sgn}(x-x'),\ [\phi_n(t,x),\phi_n(t,x')] \\ &= i\pi\ \mathrm{sgn}(x-x'),\ [\phi_c(t,x),\phi_n(t,x')] = 0.\end{aligned} \tag{D10}$$

Next, we assume that electrons can tunnel between two edges, and the tunneling Hamiltonian takes the form of

$$H_{\mathrm{tunnel}} = -t_\perp \int dt\,dx[\hat{\psi}_1^\dagger\hat{\psi}_2 + \mathrm{H.c.}], \tag{D11}$$

where $\hat{\psi}_{I=1,2}$ are the electron operators and satisfy the usual fermionic anticommutation relation. The relationship between the electron operators $\hat{\psi}_I$ and the chiral boson fields $u_I(t,x)$ is [60]

$$\begin{aligned}\hat{\psi}_1^\dagger &= \eta e^{iu_1(t,x)} = \eta e^{i(\sqrt{2}\phi_c-\phi_n)}, \\ \hat{\psi}_2^\dagger &= \eta e^{iu_2(t,x)} = \eta e^{i(\sqrt{2}\phi_c+\phi_n)},\end{aligned} \tag{D12}$$

where we have used Eq. (D8) and η is a constant depending on the cutoff. Then, the total Hamiltonian can be expressed as

$$\begin{aligned} H &= H_{\mathrm{edge}} + H_{\mathrm{tunnel}} = H_c + H_n, \\ H_c &= \frac{1}{4\pi}\int dt\,dx\ v_c(\partial_x\phi_c)^2, \\ H_n &= \frac{1}{4\pi}\int dt\,dx[v_n(\partial_x\phi_n)^2 - t_\perp'(e^{2i\phi_n} + \mathrm{H.c.})], \end{aligned}$$

where $t_\perp'$ is a constant proportional to $t_\perp$. One can see that the tunneling only appears in the neutral mode Hamiltonian H_n.

The next important step is to fermionize H_n by a Dirac fermion field $\psi_D \equiv \frac{1}{\sqrt{2\pi}}e^{i\phi_n}$, which can be further decomposed in terms of two chiral Majorana fermion fields $\chi_{i=1,2}$ [29] by $\psi_D = \frac{1}{\sqrt{2}}(\chi_1 + i\chi_2)$. Finally, we have

$$H_n = -\frac{i}{2}\int dt\,dx[(v_n - t_\perp'')\chi_1\partial_x\chi_1 + (v_n + t_\perp'')\chi_2\partial_x\chi_2], \tag{D13}$$

where $t_\perp''$ is a rescaled tunneling strength. Now, two Majorana fields are decoupled with different velocities modified by the tunneling. The key observation is, when the condition $v_n - t_\perp'' = 0$ is satisfied, one Majorana field χ_1 vanishes, leading to

$$H = \int dt\,dx\left[-\frac{i}{2}(v_n + t_\perp'')\chi_2\partial_x\chi_2 + \frac{1}{4\pi}v_c(\partial_x\phi_c)^2\right]. \tag{D14}$$

Physically, it means one Majorana mode can be completely gapped out with the help of the tunneling effect. The remaining edge theory includes a chiral boson (charged mode ϕ_c) with central charge $c_\phi = 1$, and a chiral Majorana fermion (neutral mode χ_1) with central charge $c_\chi = \frac{1}{2}$. Thus, the total central charge of remaining system is $c_{\mathrm{eff}} = c_\phi + c_\chi = 1 + \frac{1}{2}$, which is consistent with the expectation of the MR Pfaffian state.

3. Effective theory in the thin-torus limit

In this section, we study the quantum phase transition from the (331) Halperin state to the MR Pfaffian state driven by the interlayer tunneling from a different perspective. That is, we will derive an effective theory for the underlying quantum phase transition in the thin-torus limit [30,68–70]. Unlike the effective edge theory, such kind of effective theory is constructed for the bulk and is expected to describe how the ground-state manifold evolves from the (331) degeneracy to the MR Pfaffian degeneracy.

Recall that the interaction matrix elements $V^{\sigma\sigma'}_{m_1,m_2,m_3,m_4}$ on the torus only depend on $m_1 - m_3$ and $m_1 - m_4$ [Eq. (A2)]. This allows us to reformulate the translation-invariant interaction Hamiltonian in Eq. (A1) as

$$H_{\mathrm{int}} = \sum_{\sigma,\sigma'=\uparrow,\downarrow}\sum_{i=0}^{N_s-1}\sum_{r,s} U^{\sigma\sigma'}_{r,s}\,c^\dagger_{i+s,\sigma}c^\dagger_{i+r,\sigma'}c_{i+s+r,\sigma'}c_{i,\sigma}. \tag{D15}$$

Since the single-particle LLL wave function on the torus $\psi^\sigma_j(x_\sigma,y_\sigma) = (\frac{1}{\sqrt{\pi}L_2})^{\frac{1}{2}}\sum_{n=-\infty}^{+\infty} e^{\mathrm{i}\frac{2\pi}{L_2}(j+nN_s)y_\sigma}e^{-\frac{1}{2}[x_\sigma - \frac{2\pi}{L_2}(j+nN_s)]^2}$ is localized along $x_\sigma = 2\pi j/L_2$, the separation of two consecutive orbitals, or the overlap between ψ_j and ψ_{j+1}, is controlled by a single parameter $\kappa = 2\pi/L_2$. In the thin-torus limit $L_2 \ll 1$ or $\kappa \gg 1$, the overlap between two adjacent Landau orbitals is negligible, thus, the system can be viewed as a one-dimensional chain. Because the magnitude of $U^{\sigma\sigma'}_{r,s} \propto e^{-\kappa^2(s^2+r^2)/2}$ decays exponentially when $\kappa \to \infty$, the dominated interaction Hamiltonian in the thin-torus

TABLE V. The thin-torus configurations of the (331) Halperin state, expressed in the bilayer FQH site basis (see Appendix B 2). Here, we neglect the center-of-mass degeneracy caused by the translation of each configuration.

Thin-torus configuration	(K_1,K_2)
$0\uparrow 0\downarrow\ldots 0\uparrow 0\downarrow -0\downarrow 0\uparrow\ldots 0\downarrow 0\uparrow$	(0,0)
$0\uparrow 0\downarrow\ldots 0\uparrow 0\downarrow +0\downarrow 0\uparrow\ldots 0\downarrow 0\uparrow$	$(\pi,0)$
$XX00\ldots XX00+00XX\ldots 00XX$	$(0,\pi)$
$XX00\ldots XX00-00XX\ldots 00XX$	(π,π)

limit is [69,70]

$$H_{\rm int}=\sum_{\sigma,\sigma'}\sum_{i}{\sum_{r}}' U_{r,0}^{\sigma\sigma'}n_i^{\sigma}n_{i+r}^{\sigma'}, \tag{D16}$$

where $n_i^{\sigma}=c_{i,\sigma}^{\dagger}c_{i,\sigma}$, and $\sum_r'$ means $r=0$ is excluded if $\sigma=\sigma'$. $U_{r,0}^{\sigma\sigma'}$ can be treated perturbatively with the increase of r.

The thin-torus interaction (D16) only includes exponentially decaying electrostatic terms. Once we truncate it at short ranges, the ground states at a fixed filling fraction have simple charge-density-wave patterns, i.e., the thin-torus configurations of the corresponding FQH states. Here, we give the solutions for the (331) Halperin state (Table V) and the MR Pfaffian state (Table VI) [for the MR Pfaffian state, we need a similar thin-torus analysis of its three-body parent Hamiltonian rather than (D16)], labeled by their momentum quantum numbers (K_1,K_2) (see Appendix A 2) on the torus. Actually, they are quite similar to each other, except that the (331) Halperin state takes layer indices and has one more configuration $0\uparrow 0\downarrow\ldots 0\uparrow 0\downarrow -0\downarrow 0\uparrow\ldots 0\downarrow 0\uparrow$ in the $(K_1,K_2)=(0,0)$ sector. As we will analyze in Appendix E 2, strong tunneling favors the symmetric basis $c_{m,\rm s}^{\dagger}=\frac{1}{\sqrt{2}}(c_{m\uparrow}^{\dagger}+c_{m\downarrow}^{\dagger})$. Therefore, $0\uparrow 0\downarrow\ldots 0\uparrow 0\downarrow -0\downarrow 0\uparrow\ldots 0\downarrow 0\uparrow$ vanishes at strong tunneling because both $0\uparrow 0\downarrow\ldots 0\uparrow 0\downarrow$ and $0\downarrow 0\uparrow\ldots 0\downarrow 0\uparrow$ are mapped to $0101\ldots 0101$ in the effective single-component orbitals under the symmetric basis. Other three thin-torus configurations of the (331) Halperin state are mapped to $0101\ldots 0101$, $1100\ldots 1100+0011\ldots 0011$, and $1100\ldots 1100-0011\ldots 0011$, respectively, which exactly matches the thin-torus configurations of the MR Pfaffian state. This means, at least in the thin-torus limit, interlayer tunneling is indeed a mechanism that can induce the quantum phase transition from the (331) Halperin state to the MR Pfaffian state.

Now, we start to build an effective bulk theory for the phase transition. We truncate the interaction Hamiltonian (D16) at $r=2$, and add the tunneling term, leading to the total Hamiltonian as

$$\begin{aligned}
H&=H_0+H_1+H_t,\\
H_0&=\sum_{i,\sigma}U_{1,0}^{\sigma\sigma}n_i^{\sigma}n_{i+1}^{\sigma}+\sum_{i,\sigma}U_{0,0}^{\sigma\bar{\sigma}}n_i^{\sigma}n_i^{\bar{\sigma}},\\
H_1&=\sum_{i,\sigma}U_{2,0}^{\sigma\sigma}n_i^{\sigma}n_{i+2}^{\sigma}+\sum_{i,\sigma}U_{1,0}^{\sigma\bar{\sigma}}n_i^{\sigma}n_{i+1}^{\bar{\sigma}}+\sum_{i,\sigma}U_{2,0}^{\sigma\bar{\sigma}}n_i^{\sigma}n_{i+2}^{\bar{\sigma}},\\
H_t&=-t_{\perp}\sum_i c_{i,\uparrow}^{\dagger}c_{i,\downarrow}+\text{H.c.}
\end{aligned} \tag{D17}$$

We take H_1+H_t as perturbation and construct an effective Hamiltonian in the degenerate ground-state manifold of H_0.

Note that all configurations that can be related to $0\uparrow 0\downarrow\ldots 0\uparrow 0\downarrow$ by spin flips belong to the degenerate ground-state manifold of H_0. For these configurations, if we introduce a new basis $|+\rangle_i\equiv[0\uparrow]_i,|-\rangle_i\equiv[0\downarrow]_i$ for a unit cell of two consecutive orbitals, and define $\sigma_i^x=|+\rangle_i\langle -|+|-\rangle_i\langle +|,\sigma_i^z=|+\rangle_i\langle +|-|-\rangle_i\langle -|$, we can reach an effective Hamiltonian

$$H_{\rm eff}=-J_x\sum_i\sigma_i^x+J_z\sum_i\sigma_i^z\sigma_{i+1}^z \tag{D18}$$

up to the first-order perturbation, with effective coupling $J_x\sim t_{\perp}$ and $J_z\sim(U_{2,0}^{\sigma,\sigma}-U_{2,0}^{\sigma,\bar{\sigma}})/2$. $H_{\rm eff}$ is nothing but the widely studied one-dimensional transverse field Ising model, which hosts two gapped phases [59]. The ground states are doubly degenerate for $J_x<J_z$, while there is only a unique Z_2 symmetric ground state for $J_x>J_z$. And, the two different phases are separated by a quantum critical point at $J_x=J_z$ (at zero temperature) [59]. In the $J_x/J_z\to 0$ limit, the two ground states are $|+\rangle|-\rangle\ldots|+\rangle|-\rangle=0\uparrow 0\downarrow\ldots 0\uparrow 0\downarrow$ and $|-\rangle|+\rangle\ldots|-\rangle|+\rangle=0\downarrow 0\uparrow\ldots 0\downarrow 0\uparrow$, which exactly match the (331) thin-torus configurations with $(K_1,K_2)=(0,0)$ and $(\pi,0)$ up to a superposition. In the $J_x/J_z\to\infty$ limit, the unique ground state is polarized in the x direction with the form of $\prod_i\frac{|+\rangle_i+|-\rangle_i}{\sqrt{2}}=0\to 0\to\cdots 0\to 0\to$ with $\to\equiv\uparrow+\downarrow$, which exactly matches the MR Pfaffian thin-torus configuration with $(K_1,K_2)=(\pi,0)$. This effective model indicates that the (331) configuration with $(K_1,K_2)=(0,0)$ can indeed be continuously gapped out by increasing the tunneling $t_{\perp}$. To numerically verify the above picture, we calculate the energy spectrum of the one-dimensional transverse Ising model in Fig. 8. We find that, for a finite system, one of lowest-energy states (labeled by red cross) is continuously gapped out by increasing J_x, and the excitation gap at $J_x=J_z$ does not vanish (please also see the comments below). These features are very similar to what we find in Fig. 2 (main text).

In addition, all configurations that are related to $\uparrow\downarrow 00\ldots\uparrow\downarrow 00$ by simultaneously flipping two nearest-neighbor spins also belong to the degenerate ground-state manifold of H_0. For these configurations, we can introduce a new basis $|+\rangle_i\equiv[\uparrow\downarrow 00]_i,|-\rangle_i\equiv[\downarrow\uparrow 00]_i$ for a unit cell of four consecutive orbitals, and define $\sigma_i^x=|+\rangle_i\langle -|+|-\rangle_i\langle +|,\sigma_i^z=|+\rangle_i\langle +|-|-\rangle_i\langle -|$. The second-order perturbation leads to an effective Hamiltonian $H_{\rm eff}=-J_x\sum_i\sigma_i^x$ with $J_x\sim 2t_{\perp}^2/U_{1,0}^{\sigma\sigma}$. Therefore, there is no phase transition and the ground state is always $\prod_i\frac{|+\rangle_i+|-\rangle_i}{\sqrt{2}}=XX00\ldots XX00$. The same conclusion also holds for those configurations that are related to

TABLE VI. The thin-torus configurations of the MR Pfaffian state, expressed in the single-component FQH orbital basis. Here, we neglect the center-of-mass degeneracy caused by the translation of each configuration.

Thin-torus configuration	(K_1,K_2)
$0101\ldots 0101$	$(\pi,0)$
$1100\ldots 1100+0011\ldots 0011$	$(0,\pi)$
$1100\cdots 1100-0011\ldots 0011$	(π,π)

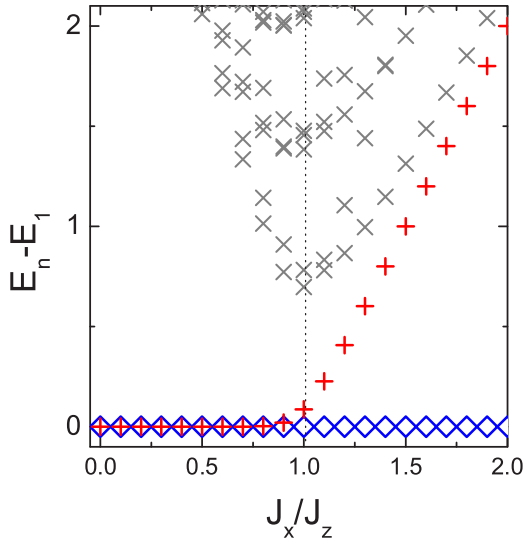

FIG. 8. Energy spectra of the one-dimensional transverse field Ising model as a function of parameter J_x/J_z. Here, the calculation is performed on a spin chain with 18 sites. It is clear that, as increasing J_x, one ground state is continuously gapped out (labeled by red cross). Please note that the evolution of the low-energy spectrum versus J_x is very similar to that in our bilayer FQH system [Fig. 2(a)]. Dotted line indicates the transition point predicted by analytic result. Please see Ref. [59] for detailed analysis of the transition in Ising model.

$00\uparrow\downarrow\ldots00\uparrow\downarrow$ by simultaneously flipping two nearest-neighbor spins. Therefore, the (331) degeneracy in the $(0,\pi)$ and (π,π) sectors cannot be changed by the tunneling.

We have clarified that the (331) Halperin state and the MR Pfaffian state are separated by a quantum critical point and the ground-state degeneracy can be reduced from fourfold to threefold. To further elucidate the "topological" property of this phase transition, we refer to the fermionic representation of the transverse field Ising model. After the Wigner-Jordan transformation, one-dimensional transverse field Ising model can be mapped to Kitaev chain model. Thus, we reach an intriguing connection here: the quantum phase transition from the (331) Halperin state to the MR Pfaffian can be understood as a transition from the weak p-wave pairing regime to the strong p-wave pairing regime. The same statement was predicted years ago [17], where Read and Green derived it by setting up the BCS effective quasiparticle Hamiltonian and Bogoliubov transformation. Here, we reach the same conclusion through the perturbation theory in the thin-torus limit. In our approach, the nature of transition becomes transparent through mapping the bilayer system to an exactly solvable model.

We would like to end this section by a comment on the validity of the thin-torus consideration. As shown above, the mapping in the thin-torus limit to an effective one-dimensional transverse Ising chain indeed provides a natural understanding of the continuous phase transition from the (331) state to the MR state which occurs in our two-dimensional bilayer system. However, whether such an effective one-dimensional model can capture other features of the original system is unknown. For example, the excitation gap of the one-dimensional transverse Ising model should close at $J_x = J_z$ in the thermodynamic limit [59]. On the contrary, we did not observe an obvious decay of the excitation gap with the system size at the critical $t_\perp$ (Fig. 4). However, we still cannot rule out the possibility that our bilayer system is also gapless at the transition point in the thermodynamic limit.

APPENDIX E: ENERGY SPECTRA FROM EXACT DIAGONALIZATION

1. Bilayer system

In the main text, we show the energy spectra of $N_e = 12$ on the torus obtained by DMRG. Here, we would like to present the torus energy spectra of smaller systems that can be reached by exact diagonalization (ED). In our bilayer FQH system, the Hilbert space grows very fast with the increase of the system size, so ED calculations are strongly limited.

In Fig. 9, we show the energy spectra of $N_e = 8$ and 10 as a function of the tunneling strength. For $N_e = 8$, with increasing the tunneling strength, one state in the momentum sector $K = 1$ comes down and eventually forms a gapless branch in the low-energy spectrum. A similar situation occurs also for $N_e = 10$. This is the main reason that previous studies

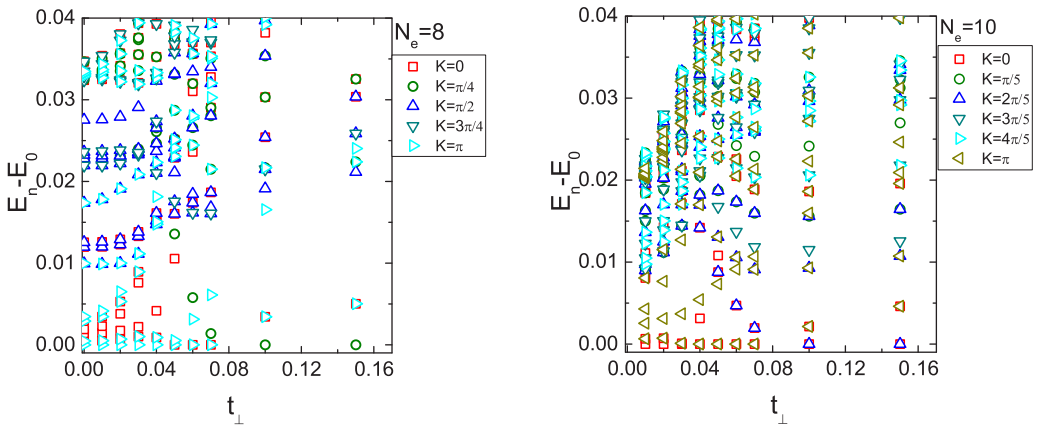

FIG. 9. Energy spectra as a function of tunneling $t_\perp$ on a square torus with $N_e = 8$ (left) and 10 (right) electrons obtained by exact diagonalization. Different momentum sectors are labeled by different symbols. All calculations are performed at layer width $w = 1.5$ and layer distance $d = 3.0$.

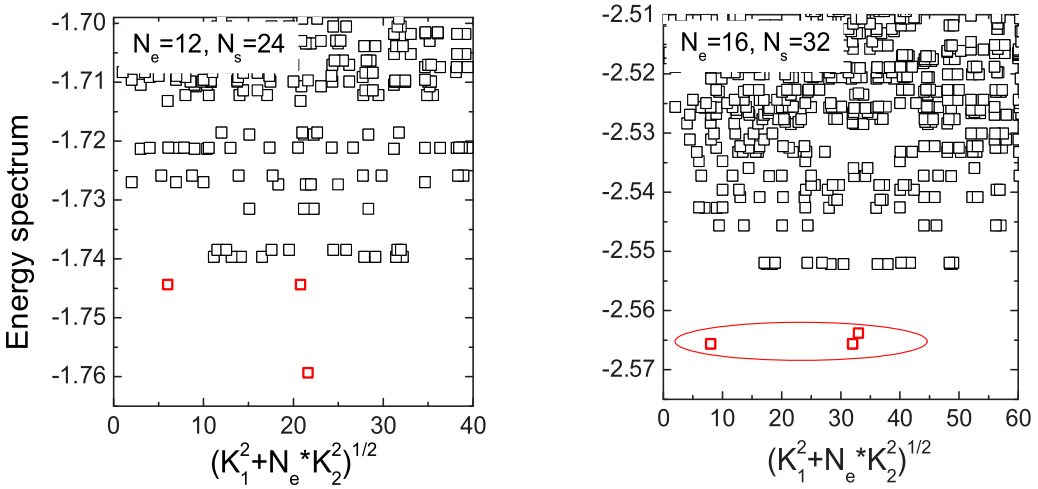

FIG. 10. Energy spectra in the strong-tunneling limit for (left) $N_e = 12$ and (right) $N_e = 16$ on the square torus obtained by ED. Energy eigenstates are labeled by a $\sqrt{K_1^2 + N_e K_2^2}$ (in unit of $2\pi/N_s$), where (K_1, K_2) is two-dimensional momentum (see Appendix A). The threefold ground-state degeneracy in $(0,\pi),(\pi,0),(\pi,\pi)$ is labeled by red squares. All calculations are performed at layer distance $d = 3.0$ and layer width $w = 1.5$.

ruled out the possibility of the MR Pfaffian state on the torus [39]. Moreover, in Fig. 9, the energy spectra at small tunneling even fail to develop stable fourfold ground-state degeneracy of the (331) Halperin state. Therefore, we believe that ED calculations suffer from finite-size effect too strongly to demonstrate the MR Pfaffian physics.

2. Effective single-component systems in the strong-tunneling limit

We can reformulate the bilayer FQH system in a new single-particle basis defined by $c^\dagger_{m,\mathrm{s}} = \frac{1}{\sqrt{2}}(c^\dagger_{m\uparrow} + c^\dagger_{m\downarrow})$ and $c^\dagger_{m,\mathrm{as}} = \frac{1}{\sqrt{2}}(c^\dagger_{m\uparrow} - c^\dagger_{m\downarrow})$, where $c^\dagger_{m,\mathrm{s}}$ ($c^\dagger_{m,\mathrm{as}}$) creates an electron in the symmetric (antisymmetric) orbital m between two layers. In this picture, the tunneling term becomes diagonal as $-t_\perp \sum_{m=0}^{N_s-1}(c^\dagger_{m,\mathrm{s}}c_{m,\mathrm{s}} - c^\dagger_{m,\mathrm{as}}c_{m,\mathrm{as}})$. Therefore, in the strong-tunneling limit $t_\perp \to \infty$, the degrees of freedom in the antisymmetric basis are frozen, thus, we can view the bilayer system as an "effective" single-component system in the symmetric basis with an average interaction $\frac{1}{2}(H_{\mathrm{intralayer}} + H_{\mathrm{interlayer}})$. This greatly simplifies the problem and makes $N_e = 12$ and 16 accessible in ED.

In Fig. 10, we show the energy spectra of $N_e = 12$ and 16 in this strong-tunneling limit on the torus obtained by ED. There are three ground states in $(K_1, K_2) = (0,\pi),(\pi,0),(\pi,\pi)$. We have one remark on the ED calculation. In the strong-tunneling limit, since the system is effectively single component, there is an exact particle-hole symmetry in the half-filled lowest Landau level (while this symmetry is explicitly broken in weak- or intermediate-tunneling regime of bilayer FQH systems). An conventional view is that there should be another copy of the MR Pfaffian degeneracy in the energy spectrum contributed by the particle-hole conjugate of the MR Pfaffian state, i.e., the anti-Pfaffian state [72,73]. For finite-size systems, two copies (and states in each copy) are split and their eigenstates are symmetric and antisymmetric linear combinations of the MR Pfaffian and anti-Pfaffian states. Apparently, Fig. 10 shows that splitting between the symmetric and antisymmetric combinations is not negligible, indicating that the ED calculation still suffers from strong finite-size effect in the strong-tunneling regime. However, we should emphasize that our main conclusion focuses on the intermediate-tunneling regime based on DMRG.

APPENDIX F: EXPERIMENTAL SETUP

1. Related experimental parameters

In this section, we briefly review some details of quantum Hall experiments in double quantum well and single wide quantum well systems. In these systems, several physical quantities are tunable in experiments, including the interlayer separation d (in unit of ℓ), interlayer tunneling strength $t_\perp$ (in unit of e^2/ℓ), and the layer width of a single quantum well w (in unit of ℓ). Different samples can be constructed with different values of d and w. Tunneling strength is determined by the height of the potential barrier between two layers in double quantum well systems or the single-particle wave-function overlap in single wide quantum well systems. Tuning the parameters can be achieved by varying the electron density ρ, which leads to the change of the effective ℓ at a fixed filling ν via the relation $\rho = \nu/2\pi\ell^2$. This allows d/ℓ, w/ℓ, and $t_\perp/(e^2/\ell)$ to be tuned continuously in a single sample.

TABLE VII. Typical parameter values for several existing quantum Hall experiments at $\nu_T = \frac{1}{2}$. The estimation of layer separation d (in unit of magnetic length ℓ), quantum well layer width w (in unit of ℓ), and tunneling strength $t_\perp$ (in unit of Coulomb energy e^2/ℓ) are taken from self-consistent calculations [22].

Experiment (Ref.)	d/ℓ	$t_\perp/(e^2/\ell)$	w/ℓ
Suen *et al.* [19,21]	4.5–7.0	0.04–0.10	2.4–2.5
Eisenstein *et al.* [20]	2.4–3.6	0.01	1.8
Shabani *et al.* [22]	5.0–8.0	0.05–0.16	2.8–3.2

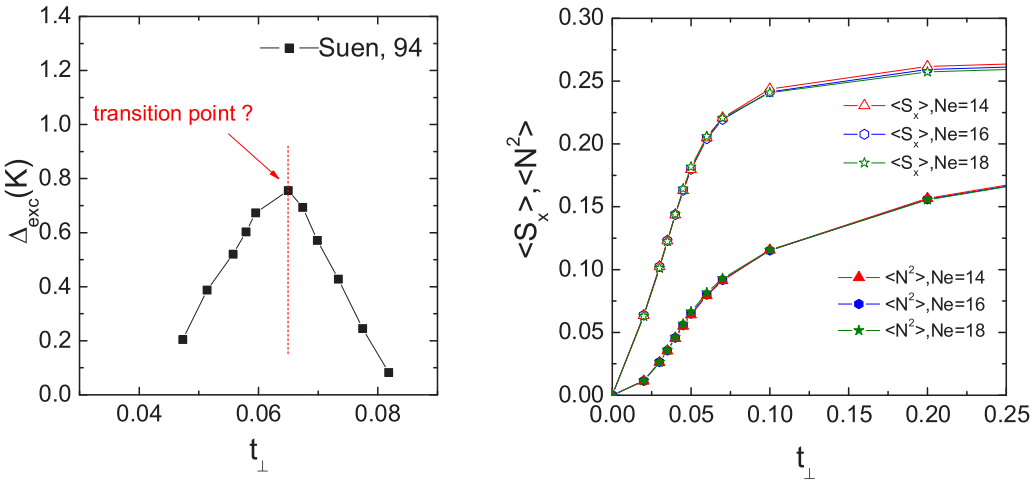

FIG. 11. (Left) The experimental observed quasiparticle excitation gaps Δ_{exc} (in unit of Kelvin) versus the tunneling strength $t_\perp$. The data are obtained from Ref. [21]. (Right) The tunneling current and particle-number fluctuation of each layer as a function of $t_\perp$ with layer width $w = 1.5$ and layer separation $d = 3.0$, which can be used to distinguish a two-component state from a single-component state.

To illustrate the typical parameter range that can be accessed, we show the parameters in several experiments at $\nu_T = \frac{1}{2}$, as shown in Table VII. In double quantum well systems [20], it is possible to vary d in the range $2 \sim 4$, while the interlayer tunneling $t_\perp$ can be suppressed to ~ 0.01. The width of individual layers in this case is less than d. On the other hand, in wide quantum wells, the effective layer distance can be varied from 2.0 to 8.0 [22], and the tunneling strength $t_\perp$ typically varies between 0.0 and 0.2. For systems where FQH can be observed, the estimated layer width w is typically much smaller than d.

2. Related experimental measurements

We briefly discuss the experimentally related observations. First of all, we emphasize that the evolution of excitation gap Δ_{exc} with tunneling strength $t_\perp$ is qualitatively consistent with the experimental observations. As shown in Fig. 11 (left), by tuning the effective tunneling strength $t_\perp$, the measured quasiparticle excitation gap Δ_{exc} develops an upward cusp behavior. Compared with our results in Fig. 4(c) in the main text, we conclude that the presence of a maximum in excitation gap in the existing experiment [21] is a direct signal of the phase transition from the (331) Halperin state to the MR Pfaffian state.

Next, we propose several methods to distinguish the (331) Halperin state and the MR Pfaffian state in experiments. First, the (331) Halperin state has a quantized drag Hall conductance $\sigma^{xy}_{\rm drag} = -\frac{e^2}{8h}$, but the drag Hall conductance of the MR Pfaffian state is not quantized. Therefore, we can measure $\sigma^{xy}_{\rm drag}$ to distinguish them. If there are separate electric contacts in two different layers, and the electric current $\delta I_\uparrow$ is forced to flow in the top layer (also called the driving layer), a measurable voltage drop $\delta V_\downarrow$ will be induced in the bottom layer (called the drag layer). On the other hand, one can also measure the tunneling current $j_t \propto \langle S_x \rangle = \frac{1}{N_\phi} \sum_i \langle c^\dagger_{i,\uparrow} c_{i,\downarrow} + \text{H.c.} \rangle$ to distinguish these two states. For the (331) Halperin state, the tunneling current between two layers should be small and sensitive to the change of the tunneling strength, as shown in Fig. 11 (right). On the contrary, the tunneling current keeps finite and almost does not change for the MR Pfaffian state. Moreover, the (331) Halperin state and the MR Pfaffian state can also be distinguished by measuring the particle-number fluctuation $\langle N^2 \rangle = \langle \delta N^2 \rangle / N_e = \langle (N_\uparrow - N_e/2)^2 \rangle / N_e = \langle (N_\downarrow - N_e/2)^2 \rangle / N_e$ in each layer. Since electrons are confined in two layers in the (331) Halperin state, the particle-number fluctuation should be strongly suppressed. But, a large particle-number fluctuation is expected for the MR Pfaffian state due to the tunneling effect, as shown in Fig. 11 (right).

[1] D. C. Tsui, H. L. Stormer, and A. C. Gossard, Phys. Rev. Lett. **48**, 1559 (1982).
[2] R. B. Laughlin, Phys. Rev. Lett. **50**, 1395 (1983).
[3] X. G. Wen, Int. J. Mod. Phys. B **04**, 239 (1990).
[4] G. Moore and N. Read, Nucl. Phys. B **360**, 362 (1991).
[5] M. Greiter, X.-G. Wen, and F. Wilczek, Phys. Rev. Lett. **66**, 3205 (1991).
[6] N. Read and E. Rezayi, Phys. Rev. B **59**, 8084 (1999).
[7] C. Nayak, S. H. Simon, A. Stern, M. Freedman, and S. Das Sarma, Rev. Mod. Phys. **80**, 1083 (2008).
[8] R. Willett, J. P. Eisenstein, H. L. Störmer, D. C. Tsui, A. C. Gossard, and J. H. English, Phys. Rev. Lett. **59**, 1776 (1987).
[9] W. Pan, J.-S. Xia, V. Shvarts, D. E. Adams, H. L. Stormer, D. C. Tsui, L. N. Pfeiffer, K. W. Baldwin, and K. W. West, Phys. Rev. Lett. **83**, 3530 (1999).
[10] I. P. Radu, J. B. Miller, C. M. Marcus, M. A. Kastner, L. N. Pfeiffer, and K. W. West, Science **320**, 899 (2008).
[11] M. Dolev, M. Heiblum, V. Umansky, A. Stern, and D. Mahalu, Nature (London) **452**, 829 (2008).

[12] R. L. Willett, C. Nayak, K. Shtengel, L. N. Pfeiffer, and K. W. West, Phys. Rev. Lett. **111**, 186401 (2013).
[13] S. Baer, C. Rössler, T. Ihn, K. Ensslin, C. Reichl, and W. Wegscheider, Phys. Rev. B **90**, 075403 (2014).
[14] B. I. Halperin, Helv. Phys. Acta **56**(1-3), 75 (1983).
[15] F. D. M. Haldane and E. H. Rezayi, Phys. Rev. Lett. **60**, 956 (1988).
[16] X.-G. Wen, Phys. Rev. Lett. **84**, 3950 (2000).
[17] N. Read and D. Green, Phys. Rev. B **61**, 10267 (2000).
[18] M. Barkeshli and X.-G. Wen, Phys. Rev. B **84**, 115121 (2011).
[19] Y. W. Suen, L. W. Engel, M. B. Santos, M. Shayegan, and D. C. Tsui, Phys. Rev. Lett. **68**, 1379 (1992).
[20] J. P. Eisenstein, G. S. Boebinger, L. N. Pfeiffer, K. W. West, and S. He, Phys. Rev. Lett. **68**, 1383 (1992).
[21] Y. W. Suen, H. C. Manoharan, X. Ying, M. B. Santos, and M. Shayegan, Phys. Rev. Lett. **72**, 3405 (1994).
[22] J. Shabani, Y. Liu, M. Shayegan, L. N. Pfeiffer, K. W. West, and K. W. Baldwin, Phys. Rev. B **88**, 245413 (2013).
[23] J. Eisenstein, Annu. Rev. Condens. Matter Phys. **5**, 159 (2014).
[24] M. Greiter, X. G. Wen, and F. Wilczek, Phys. Rev. B **46**, 9586 (1992).
[25] T.-L. Ho, Phys. Rev. Lett. **75**, 1186 (1995).
[26] C. Nayak and F. Wilczek, Nucl. Phys. B **479**, 529 (1996).
[27] E. Fradkin, C. Nayak, and K. Schoutens, Nucl. Phys. B **546**, 711 (1999).
[28] A. Cappelli, L. S. Georgiev, and I. T. Todorov, Nucl. Phys. B **599**, 499 (2001).
[29] J. Naud, L. P. Pryadko, and S. Sondhi, Nucl. Phys. B **565**, 572 (2000).
[30] A. Seidel and K. Yang, Phys. Rev. Lett. **101**, 036804 (2008).
[31] N. Regnault, M. O. Goerbig, and T. Jolicoeur, Phys. Rev. Lett. **101**, 066803 (2008).
[32] B. I. Halperin, Surf. Sci. **305**, 1 (1994).
[33] T. Chakraborty and P. Pietiläinen, Phys. Rev. Lett. **59**, 2784 (1987).
[34] D. Yoshioka, A. H. MacDonald, and S. M. Girvin, Phys. Rev. B **39**, 1932 (1989).
[35] S. He, S. Das Sarma, and X. C. Xie, Phys. Rev. B **47**, 4394 (1993).
[36] M. R. Peterson and S. Das Sarma, Phys. Rev. B **81**, 165304 (2010).
[37] K. Nomura and D. Yoshioka, J. Phys. Soc. Jpn. **73**, 2612 (2004).
[38] Z. Papić, G. Möller, M. V. Milovanović, N. Regnault, and M. O. Goerbig, Phys. Rev. B **79**, 245325 (2009).
[39] Z. Papić, M. O. Goerbig, N. Regnault, and M. V. Milovanović, Phys. Rev. B **82**, 075302 (2010).
[40] J.-S. Jeong and K. Park, Phys. Rev. B **91**, 195119 (2015).
[41] S. R. White, Phys. Rev. Lett. **69**, 2863 (1992).
[42] N. Shibata and D. Yoshioka, Phys. Rev. Lett. **86**, 5755 (2001).
[43] A. E. Feiguin, E. Rezayi, C. Nayak, and S. Das Sarma, Phys. Rev. Lett. **100**, 166803 (2008).
[44] J. Zhao, D. N. Sheng, and F. D. M. Haldane, Phys. Rev. B **83**, 195135 (2011).
[45] M. P. Zaletel, R. S. K. Mong, F. Pollmann, and E. H. Rezayi, Phys. Rev. B **91**, 045115 (2015).
[46] J. C. Y. Teo and C. L. Kane, Phys. Rev. B **89**, 085101 (2014).
[47] A. Vaezi and M. Barkeshli, Phys. Rev. Lett. **113**, 236804 (2014).
[48] Y. Zhang and X.-L. Qi, Phys. Rev. B **89**, 195144 (2014).
[49] A. Kitaev and J. Preskill, Phys. Rev. Lett. **96**, 110404 (2006).
[50] M. Levin and X.-G. Wen, Phys. Rev. Lett. **96**, 110405 (2006).
[51] H. Li and F. D. M. Haldane, Phys. Rev. Lett. **101**, 010504 (2008).
[52] X.-G. Wen, Adv. Phys. **44**, 405 (1995).
[53] W. Zhu, S. S. Gong, F. D. M. Haldane, and D. N. Sheng, Phys. Rev. Lett. **115**, 126805 (2015).
[54] R. S. K. Mong, M. P. Zaletel, F. Pollmann, and Z. Papić, arXiv:1505.02843.
[55] Z. Liu, A. Vaezi, K. Lee, and E.-A. Kim, Phys. Rev. B **92**, 081102 (2015).
[56] S. Geraedts, M. P. Zaletel, Z. Papić, and R. S. K. Mong, Phys. Rev. B **91**, 205139 (2015).
[57] M. Milovanović and N. Read, Phys. Rev. B **53**, 13559 (1996).
[58] X.-G. Wen, Phys. Rev. Lett. **70**, 355 (1993).
[59] S. Sachdev, Science **288**, 475 (2000).
[60] X. G. Wen, Phys. Rev. B **41**, 12838 (1990).
[61] X.-G. Wen, Int. J. Mod. Phys. B **06**, 1711 (1992).
[62] E. Fradkin, *Field Theories of Condensed Matter Physics* (Cambridge University Press, Cambridge, 2013).
[63] W. Bishara, P. Bonderson, C. Nayak, K. Shtengel, and J. K. Slingerland, Phys. Rev. B **80**, 155303 (2009).
[64] G. A. Fiete, W. Bishara, and C. Nayak, Phys. Rev. Lett. **101**, 176801 (2008).
[65] M. A. Mueed, D. Kamburov, S. Hasdemir, M. Shayegan, L. N. Pfeiffer, K. W. West, and K. W. Baldwin, Phys. Rev. Lett. **114**, 236406 (2015).
[66] M. A. Mueed, D. Kamburov, L. N. Pfeiffer, K. W. West, K. W. Baldwin, and M. Shayegan, Phys. Rev. Lett. **117**, 246801 (2016).
[67] F. D. M. Haldane, Phys. Rev. Lett. **51**, 605 (1983).
[68] B. A. Bernevig and F. D. M. Haldane, Phys. Rev. Lett. **100**, 246802 (2008).
[69] E. J. Bergholtz and A. Karlhede, Phys. Rev. Lett. **94**, 026802 (2005).
[70] A. Seidel, H. Fu, D.-H. Lee, J. M. Leinaas, and J. Moore, Phys. Rev. Lett. **95**, 266405 (2005).
[71] Z. Liu, E. J. Bergholtz, H. Fan, and A. M. Läuchli, Phys. Rev. B **85**, 045119 (2012).
[72] M. R. Peterson, T. Jolicoeur, and S. Das Sarma, Phys. Rev. Lett. **101**, 016807 (2008).
[73] H. Wang, D. N. Sheng, and F. D. M. Haldane, Phys. Rev. B **80**, 241311 (2009).